

OPEN ACCESS

Modeling Polycrystalline Electrode-electrolyte Interfaces: The Differential Capacitance

To cite this article: Rüdiger Müller *et al* 2020 *J. Electrochem. Soc.* **167** 106512

View the [article online](#) for updates and enhancements.



241st ECS Meeting

May 29 – June 2, 2022 Vancouver • BC • Canada

Abstract submission deadline: Dec 3, 2021

Connect. Engage. Champion. Empower. Accelerate.
We move science forward



Submit your abstract





Modeling Polycrystalline Electrode-electrolyte Interfaces: The Differential Capacitance

Rüdiger Müller,^z  Jürgen Fuhrmann,^{ib}  and Manuel Landstorfer 

Weierstrass Institute, Mohrenstr. 39, 10117 Berlin, Germany

We present and analyze a model for polycrystalline electrode surfaces based on an improved continuum model that takes finite ion size and solvation into account. The numerical simulation of finite size facet patterns allows to study two limiting cases: While for facet size diameter $d^{\text{facet}} \rightarrow 0$ we get the typical capacitance of a spatially homogeneous but possible amorphous or liquid surface, in the limit $1[\text{nm}] \ll d^{\text{facet}}$, an ensemble of non-interacting single crystal surfaces is approached. Already for moderate size of the facet diameters, the capacitance is remarkably well approximated by the classical approach of adding the single crystal capacities of the contributing facets weighted by their respective surface fraction. As a consequence, the potential of zero charge is not necessarily attained at a local minimum of capacitance, but might be located at a local capacitance maximum instead. Moreover, the results show that surface roughness can be accurately taken into account by multiplication of the ideally flat polycrystalline surface capacitance with a single factor. In particular, we find that the influence of the actual geometry of the facet pattern in negligible and our theory opens the way to a stochastic description of complex real polycrystal surfaces.

© 2020 The Author(s). Published on behalf of The Electrochemical Society by IOP Publishing Limited. This is an open access article distributed under the terms of the Creative Commons Attribution 4.0 License (CC BY, <http://creativecommons.org/licenses/by/4.0/>), which permits unrestricted reuse of the work in any medium, provided the original work is properly cited. [DOI: 10.1149/1945-7111/ab9cca]



Manuscript submitted April 29, 2020; revised manuscript received May 27, 2020. Published June 24, 2020.

Supplementary material for this article is available [online](#)

The theoretical and experimental investigation of polycrystalline electrode surfaces provides valuable information for the understanding of the performance for many types of real electrochemical devices. Fundamental concepts like the structure of the electrochemical double layer, double layer capacitance, Faradaic reaction rate equations and others have been derived and verified experimentally for single crystal or liquid metal electrodes, see e.g.^{1–3} In either case, the physicochemical properties of these electrodes surfaces can be idealized as entirely homogeneous. In contrast, real solid metal electrodes are most often polycrystalline. Surfaces of polycrystalline electrodes in general exhibit a complex unstructured and random pattern of facets with different crystallographic orientation as sketched in Fig. 2 left. It is well known that the electron work function depends on the crystallographic orientation of a surface.^{4,5} As a consequence, the differential capacity and the corresponding potential of zero charge (PZC) of the surface in contact to an electrolyte depend on the crystallographic orientation as well, cf.^{6–8}

In this paper we propose a mathematically sound approach which allows to derive characteristics of polycrystalline electrodes from a thermodynamically well founded model. We focus on double layer capacitance and potential of zero charge as equilibrium properties. In particular, we aim at the characterization of an *ideal polycrystalline surface* where typical facet size, characterized by the diameter d^{facet} , is large compared to a suitable reference length of the electrolyte. Here we always set the reference length for an aqueous electrolyte to $1[\text{nm}]$. For the ideal polycrystalline surface, the influence of edge effects related to facet boundaries can be neglected such that compact asymptotic equations defining potential of zero charge and potential dependent double layer capacitance can be derived. Numerical simulations of the spatial charge distribution in the boundary layers confirm that contributions from facet boundary effects indeed are marginal. Ultimately, we replace discrete facet configurations by probability distributions of facets with identical physical properties. This allows a very compact reformulation of the polycrystalline electrode properties in terms of convolution integrals.

The development of the classical Gouy-Chapman-Stern-Grahame theory of the electrochemical double layer^{9,10} strongly relied on experimental measurements at mercury electrodes. Since these electrodes consist of a liquid metal, their clean surface in contact with an electrolyte typically can be considered as ideally smooth and

physical homogeneous. Thus, when trying to transfer the theory from liquid to solid metal electrodes, first an awareness about the relevance of surface roughness and individual properties of surfaces facets of different crystallographic orientation needed to be established, cf.¹¹ Valette and Harmelin¹² first related careful capacity measurements of silver single crystal surfaces with the corresponding experimental results for polycrystalline silver electrodes. Although not explicitly written in Ref. 12, a relation for the capacity of the polycrystalline surface was assumed that is the same as the limiting Eq. 3 below. In Ref. 13 different equivalent circuits for the representation of polycrystalline surfaces are proposed and analyzed by comparison with experimental data. The comparison supported a model related to Eq. 3. In Ref. 14 the range of applicability of 3 is discussed based on a spatially resolved analysis according to the Gouy-Chapman-Stern-Grahame model in Ref. 15. Moreover, it was shown that in the limit of vanishing size of the facets, the alternative equivalent circuit model of Ref. 13 is approached.

To describe a polycrystalline electrode-electrolyte interface, we apply in this work a model on the basis of continuum non-equilibrium thermo-electrodynamics that was derived and analyzed in Refs. 16–19. For a review of the prior development of generalized Nernst-Planck models, we refer to Ref. 20. The model applied here incorporates the pressure in the electrolyte as a variable and the momentum balance, which ensures thermodynamic consistency. Further, it allows to account for volume exclusion effects of all species, and especially of the solvation effect. In Ref. 17 it has been shown that this model is capable to predict qualitatively and in the correct quantitative range the differential capacity of single crystal electrodes with respect to the applied voltage and with respect to the salt concentration. For further discussion of the underlying model, we refer to the supplementary material (available online at stacks.iop.org/JES/167/106512/mmedia). For a single crystal electrode in contact with a non-adsorbing electrolyte, the capacity is exclusively due to the charging of the double layer. As long as the bulk electrolyte concentration is not too large, it shows the typical symmetric camel shape capacitance curve. Figure 1 (left) demonstrates the good agreement between the model predictions and the experimental measurements. The potential of zero charge (PZC) is located at the local capacity minimum and does not change with salt concentration. The absolute value of the PZC depends on the crystallographic orientation of the metal surface. Between differently oriented surfaces, the difference of their respective PZC values are known to correspond well to the differences of the electron work

^zE-mail: Ruediger.Mueller@wias-berlin.de

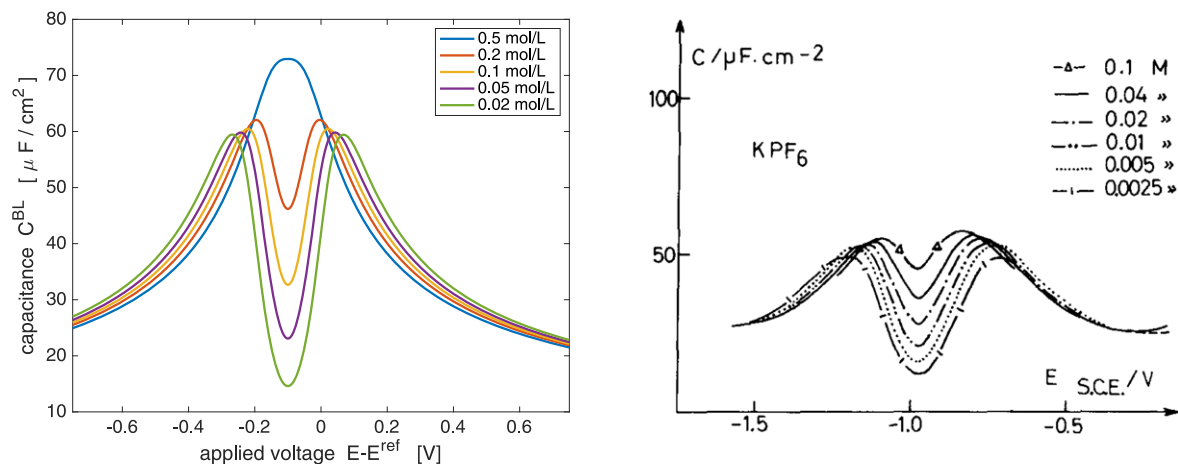


Figure 1. Left: Computed boundary layer capacity of a single crystal surface for different concentrations of a non-adsorbing electrolyte. Right: Measured capacitance at a (110) surface of Ag (Fig. 3a of Ref. 6, reprinted the permission of Elsevier).

function.^{5,17} In addition, we can observe in Fig. 1 (left) the expected behavior such that for increasing bulk salt concentration the local minimum at the PZC becomes less deep and eventually vanishes, leading to a single maximum capacity curve.

For a polycrystalline electrode surface, we derive expressions of the double layer charge, the potential of zero charge, and the differential capacitance and compare these to the (theoretically) more simple and well understood case of single crystal surfaces. Within some reasonable scaling it is a remarkable and non-obvious feature of the resulting model that double layer charge, and subsequently the potential of zero charge, as well as the differential capacity can be determined from solutions of an algebraic equation system, rather than solving space dependent differential equations. This even holds true for a stochastic description of a polycrystalline electrode surface, which we show within this work.

The inhomogeneity of the surface capacitance is commonly believed to cause so called “frequency dispersion” in electrochemical impedance spectroscopy, cf.,²¹ and the effects of surface inhomogeneity can be expected to have even more serious impact in the presence of Faradaic reactions. We plan to investigate these non-equilibrium aspects in follow-up research.

Outline. In the next section, we give a brief overview over our general approach and the main results. Next, we summarize the general equilibrium conditions of the applied continuum model and appropriate material models from Refs. 17, 19. In the following, we apply the model to solid electrode surfaces. The differential capacity of a single crystal surface is introduced and a model for polycrystalline surfaces is developed. Then, there is a section devoted to an assessment of the results obtained by numerical solution of the boundary value problem in 2D and in 3D for periodically patterned surfaces of finite size facets. In particular, the limiting behavior for extreme facet size parameters and the influence of surface roughness on the length scale of the facets are analyzed. We proceed with a discussion of the polycrystal model in the case of large facet size, including the effects of adsorption and the stochastic description of polycrystalline surfaces. We close with some concluding remarks.

General Approach and Main Results

We model the polycrystalline electrode surface by a regular surface pattern with $N > 1$ different types of facets. Each facet corresponds to certain crystallographic orientation. To each facet Σ_i , $1 \leq i \leq N$, we assign a value of the electron work function and its surface fraction $s_i = \frac{|\Sigma_i|}{|\Sigma|}$ with $\sum_{i=1}^N s_i = 1$, where $|\cdot|$ denotes the surface area. We show, based on our thermodynamic model of Section 3, that the electric potential φ^i on each facet Σ_i is related to the work function, or in our notation², to the chemical potential μ_e^i of surface electrons of the respective surface orientation.⁵ The

polycrystalline electrode surface $\Sigma = \cup_i \Sigma_i$ is then considered to be in contact to some electrolytic solution in the volume domain Ω^E . The electrolyte in thermodynamic equilibrium is described by an improved Poisson-Boltzmann system⁴, i.e. the system

$$-\varepsilon_0 \operatorname{div}(1 + \chi) \nabla \varphi = q(\varphi, p), \quad \sum_{\alpha \in \mathcal{I}_E} y_\alpha(\varphi, p) = 1, \quad [1]$$

where y_α refers to the species mole fractions and p is the pressure. On the electrode surface, facet-wise constant boundary values for the electric potential are prescribed. Then, the adjacent space charge layer in the electrolyte can be computed numerically. Figure 2 (right, bottom) shows a typical 3D numerical computation of the electric potential iso-surfaces in the electrolyte Ω^E for a periodical checker-board electrode surface. Based on such numerical solution we can compute, (i) the overall double layer charge Q_{poly} as function of the applied voltage E , (ii) the potential of zero charge E^{PZC} of a polycrystalline electrode-electrode interface, and (iii) the corresponding double layer capacity C_{poly} (see Fig. 2 (right, top)). This approach is valid for arbitrary geometries and facet sizes. The only assumption here is that the intersecting lines between two facets do not have independent thermodynamic quantities.

For a non-adsorbing electrolyte^b we have in general

$$(M0) \quad \begin{cases} Q_{\text{poly}} = \frac{1}{|\Sigma|} \int_{\Omega^E} q(x) dx = Q_{\text{poly}}^{\text{BL}}(E) \\ E_{\text{poly}}^{\text{PZC}} = E \quad \text{s.t.} \quad Q_{\text{poly}}^{\text{BL}}(E) \stackrel{!}{=} 0 \\ C_{\text{poly}} = \frac{dQ_{\text{poly}}^{\text{BL}}(E)}{dE} =: C_{\text{poly}}^{\text{BL}}(E) \end{cases} \quad [2]$$

subject to the coupled equation system 1.

A scale analysis of the boundary value problem yields two characteristic length scales of the model: the typical diameter d^{facet} of the facets Σ_i and a reference length L^{ref} related to the non-dimensionalization of the Poisson equation in 1. This reference length is in the order of the Debye length L^{Debye} of the electrolyte, however, independent of the bulk electrolyte concentration. We found that $L^{\text{ref}} = 1[\text{nm}]$ is a proper scaling for for aqueous solutions, which is used throughout the manuscript.

If the facet or facet diameter d^{facet} is large compared to $1[\text{nm}]$, the double layer charge Q_{poly} can be obtained as a sum of the single facet boundary layer charges Q^{BL} , weighted by their respective surface fraction s_i . Subsequently, the potential of zero charge $E_{\text{poly},\infty}^{\text{PZC}}$ can be

^aCompared to the standard Poisson-Boltzmann equation, the charge density q in 1 does not only depend on the electric potential ϕ , but also on the pressure p and the Poisson equation is additionally coupled to an algebraic equation.

^bNote that specific adsorption is also discussed within this work.

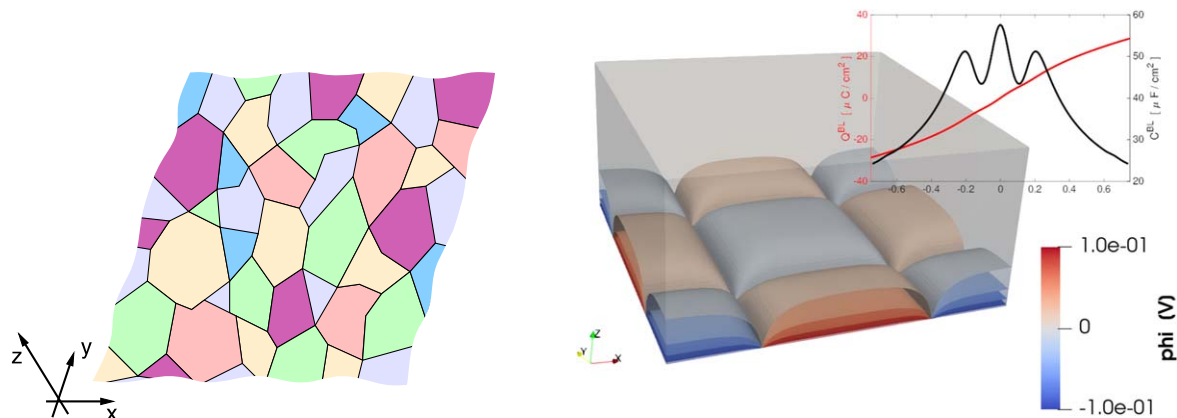


Figure 2. Sketch of the facet structure of a polycrystalline surface (left) and isosurfaces of the electric potential in the electrolyte from 3D-FEM computation (right). The surface consists of a periodic checkerboard pattern of equally sized facets. The corresponding double layer charge Q_{poly} and capacity C_{poly} as function of the applied voltage E .

determined from an algebraic equation system, and the differential capacity C_{poly} obeys also an algebraic representation, i.e.

(M1) $d^{\text{facet}} \gg 1[\text{nm}]$:

$$\begin{cases} Q_{\text{poly}} = \sum_{i=1}^N s_i \cdot \hat{Q}^{\text{BL}}\left(E + \frac{1}{e_0 s} \mu_e^i - E^{\text{ref}}\right) =: Q_{\text{poly},\infty}^{\text{BL}}(E) \\ E_{\text{poly},\infty}^{\text{PZC}} = E \quad \text{s.t.} \quad Q_{\text{poly},\infty}^{\text{BL}}(E) \stackrel{!}{=} 0 \\ C_{\text{poly}} = \sum_{i=1}^N s_i \cdot \hat{C}^{\text{BL}}\left(E + \frac{1}{e_0 s} \mu_e^i - E^{\text{ref}}\right) =: C_{\text{poly},\infty}^{\text{BL}}(E), \end{cases} \quad [3]$$

where \hat{Q}^{BL} and \hat{C}^{BL} are nonlinear functions specified in Section 3. The construction of the capacity $C_{\text{poly},\infty}^{\text{BL}}$ of a polycrystalline electrode in the case of facets with two equal surface fractions is illustrated in Fig. 3 (right). Remarkably, the potential of zero charge $E_{\text{poly},\infty}^{\text{PZC}}$ of this polycrystalline surface in this case is located at the capacity maximum and not at a local minimum of the curve!

For realistic polycrystalline electrodes, the consecutive labeling of all facets might be impractical. We propose thus a stochastic description of the surface in terms of a probability density f , modeling the surface fraction as function of the surface chemical potential of electrons. We derive in the limit $1[\text{nm}] \ll d^{\text{facet}}$ the model

(M2) $d^{\text{facet}} \gg 1[\text{nm}]$:

$$\begin{cases} Q_{\text{poly}} = (f * Q^{\text{BL}})(E) =: Q_{\text{poly},\infty}^{\text{BL}}(E) \\ E_{\text{poly},\infty}^{\text{PZC}} = E \quad \text{s.t.} \quad Q_{\text{poly},\infty}^{\text{BL}}(E) \stackrel{!}{=} 0 \\ C_{\text{poly}} = (f * C^{\text{BL}})(E) =: C_{\text{poly},\infty}^{\text{BL}}(E) \end{cases} \quad [4]$$

Figure 4 (left) shows two different distributions functions of the surface fraction and Fig. 4 (right) the corresponding differential capacitance. We observe, that a sharp peak of the distribution function leads to a capacitance close to that of a single crystal surface. More general, in Section 6.4, we see that a discrete distribution of PZC values can be well approximated by a distribution function consisting of a finite number of clearly separated peaks. Increasing the standard deviation of the normal-distribution, results in stronger smearing of the capacitance over the potential range such that the capacity minima actually disappear, while the overall shape broadens. We discuss this aspect more in detail within this work.

In the opposite limiting case of vanishing facet diameter $d^{\text{facet}} \rightarrow 0$, the potential of zero charge is given as the surface fraction weighted average of the corresponding single crystal quantities, while the charge Q_{poly} and the capacity C_{poly} remain non-linear expressions identical to the ones of a typical single crystal surface, i.e.

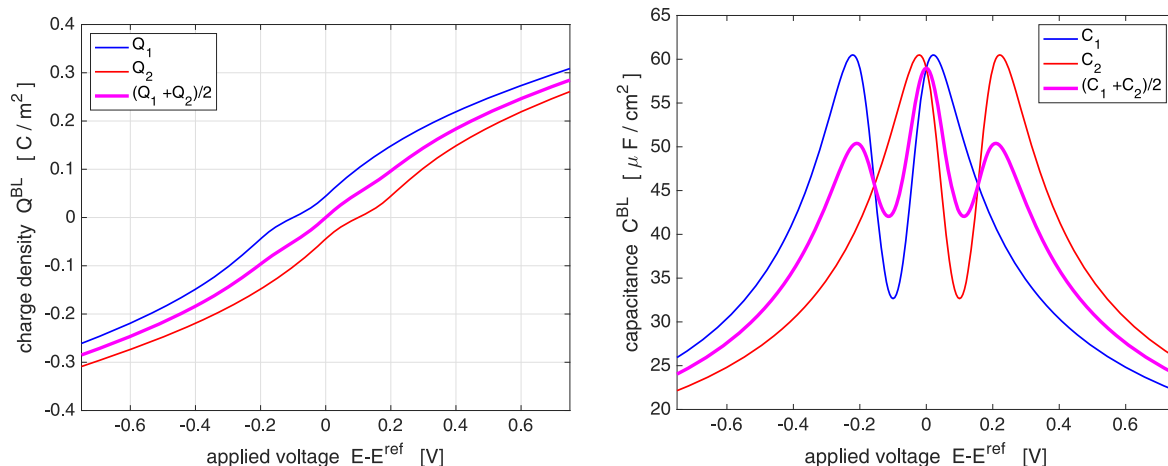


Figure 3. Double layer charge and differential capacitance of a polycrystalline electrode determined from 3 with $s_1 = s_2 = \frac{1}{2}$.

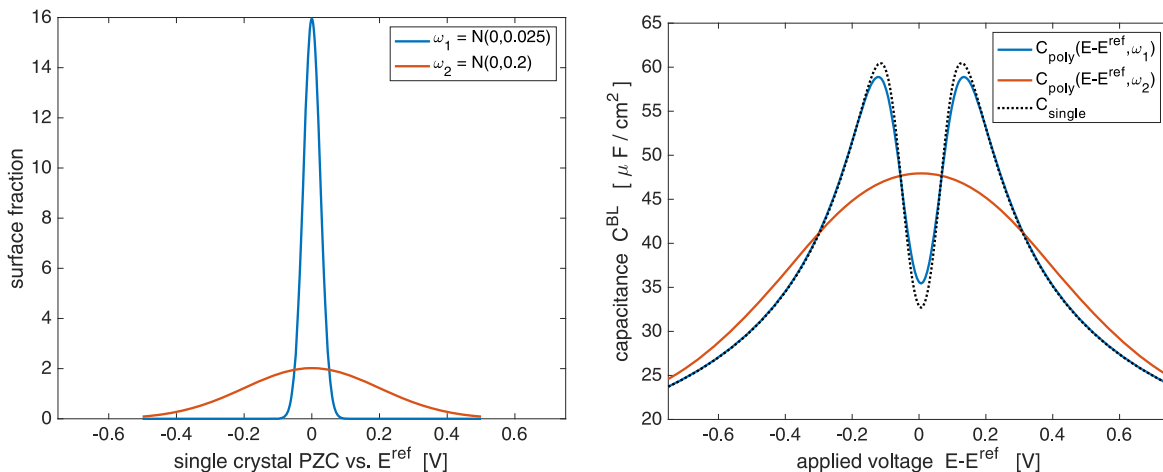


Figure 4. Left: densities of the surface chemical potential μ_e given by normal distributions with different standard deviation. Right: Capacity curves for the respective densities (solid —) and for the planar single crystal case (dotted line ...). For large σ , the the capacity has a single maximum unlike the camel shape for perturbations of the single crystal surface by small σ .

(M3) $d^{\text{facet}} \ll 1$ [nm]:

$$\begin{cases} Q_{\text{poly}} &= \hat{Q}^{\text{BL}} \left(E + \frac{1}{e_0} \sum_{i=1}^N s_i \mu_e^i - E^{\text{ref}} \right) =: Q_{\text{poly},0}^{\text{BL}}(E) \\ E_{\text{poly}}^{\text{PZC}} &= E^{\text{ref}} - \frac{1}{e_0} \sum_{i=1}^N s_i \mu_e^i|_{\Sigma_i} =: E_{\text{poly},0}^{\text{PZC}} \\ C_{\text{poly}}^{\text{BL}}(E) &= \hat{C}^{\text{BL}}(E - E_{\text{poly},0}^{\text{PZC}}) =: C_{\text{poly},0}^{\text{BL}}(E). \end{cases} \quad [5]$$

Continuum Model

We use a continuum model that is based on a coupled volume-surface description of charged and possibly reacting mixtures coupled with the electromagnetic field. Detailed description of the modeling can be found in Refs. 16, 17, 19. Following the standard approach in non-equilibrium thermodynamics, the modeling consists of two steps. The first step is universal, i.e. material independent, leading to the general model equations in Section 3.1. In the second step, which is material dependent, non-negative entropy production is guaranteed by application of an entropy principle, cf. 19. After this, specific behavior of a certain considered material is described in terms of free energy densities in each volume domain and on the surface. We summarize the free energy densities derived in Refs. 16, 17 in Section 3.2. In general these free energy densities have to be derived from models of different character on an underlying finer scale.

In this model, as a convention, each quantity defined in the volume has a corresponding quantity confined to the electrode surface Σ . We use the same letters for bulk and surface quantities and indicate the surface quantities by an underscored “s”. For a surface Σ , we choose the orientation of the a normal vector that we denote by ν . Then, we denote the adjacent bulk volumes by Ω^{E} and Ω^{M} , such that ν is the outer normal of Ω^{E} . For a generic function u in the volume, we can define the trace^e and jump at Σ by

$$u|_{\Sigma}^{\text{K}} = \lim_{x \in \Omega^{\text{K}} \rightarrow \Sigma} u(x), \quad \text{K} = \text{E}, \text{M} \quad [[u]]_{\Sigma} = u|_{\Sigma}^{\text{E}} - u|_{\Sigma}^{\text{M}}. \quad [6]$$

Bulk positions far away from the surface Σ are denoted by x^{K} and the evaluation of some function $u(x)$ the bulk points is denoted by $u^{\text{K}} = u(x^{\text{K}})$, $\text{K} = \text{E}, \text{M}$.

^eThe notation indicates that the definition can be made for both domains Ω^{E} and Ω^{M} in analogous manner. If u is not defined in either Ω^{E} or Ω^{M} , the respective trace value is set to 0.

Description of mixtures. To refer to the constituents of a mixture on the surface Σ or the adjacent volume domains Ω^{K} , we use according index sets \mathcal{I}_{Σ} , resp. \mathcal{I}_{K} of species. For each constituent, we denote the molecular mass by m_{α} , the partial molar volume by v_{α}^{ref} , the charge number by z_{α} , and the number density of particles per m^3 by n_{α} , where $\alpha \in \mathcal{I}_{\text{K}}$ or $\alpha \in \mathcal{I}_{\Sigma}$, respectively. Then, we introduce the partial mass density $\rho_{\alpha} = m_{\alpha} n_{\alpha}$. The free charge density is ($\text{K} = \text{M}, \text{E}$)

$$q = \sum_{\alpha \in \mathcal{I}_{\text{K}}} z_{\alpha} n_{\alpha}, \quad q_s = \sum_{\alpha \in \mathcal{I}_{\Sigma}} z_{\alpha} n_{\alpha}. \quad [7]$$

General assumptions. We restrict our considerations to the isothermal case, where the temperature T enters the equations only as a constant parameter and on the surface there holds $T = T|_{\Sigma}^{\text{E}} = T|_{\Sigma}^{\text{M}}$. Moreover, we only consider the electrostatic case where the electric field is given as $\mathbf{E} = -\nabla\varphi$. Excluding surface dipoles, the electric potential ϕ is continuous at the surface, i.e. we can set $\varphi = \varphi|_{\Sigma}^{\text{E}} = \varphi|_{\Sigma}^{\text{M}}$. Within this work, we assume a simple material model with a constant dielectric susceptibility χ . In the following, we neglect gravitation and restrict the presentation to planar interfaces with no tangential transport on the surface.

Model equations.—The general continuum model relies on universal, i.e. material independent balance equations in the volume domains and on the surface. However, the model equations contain several material dependent constitutive quantities which need appropriate modeling. We summarize here the equilibrium equations that result from the much more complex modeling framework.¹⁹ The key ingredients for the material modeling are the free energy densities^d $\rho\psi$, $\rho\psi_s$ in the bulk and on the volume, respectively. Due to the assumed constant dielectric susceptibility, the free energy densities are of the rather general structure

$$\begin{aligned} \rho\psi &= \rho\hat{\psi}(T, (n_{\alpha})_{\alpha \in \mathcal{I}_{\text{K}}}) - \frac{1}{2}\chi\epsilon_0|\nabla\varphi|^2, \\ \rho\psi_s &= \rho\hat{\psi}_s(T, (n_{\alpha})_{\alpha \in \mathcal{I}_{\Sigma}}). \end{aligned} \quad [8]$$

The chemical potentials are defined as

$$\mu_{\alpha} = \frac{\partial \rho\psi}{\partial n_{\alpha}}, \quad \mu_{\alpha}^s = \frac{\partial \rho\psi_s}{\partial n_{\alpha}^s}. \quad [9]$$

By means of Gibbs-Duhem relations, we introduce the material pressure p and surface tension γ as

^dWhere not necessary, we omit the labels ^E or ^M for the volume domains.

$$p = -\rho\hat{\psi} + \sum_{\alpha \in \mathcal{I}_K} n_\alpha \mu_\alpha, \quad \gamma = \rho\hat{\psi} - \sum_{\alpha \in \mathcal{I}_S} n_\alpha \mu_\alpha. \quad [10]$$

Equilibrium bulk equations. The equilibrium of an incompressible mixture in a bulk domain Ω is characterized by

$$-(1 + \chi)\varepsilon_0 \Delta \varphi = q, \quad [11a]$$

$$\nabla p = -q \nabla \varphi, \quad [11b]$$

$$0 = \nabla(\mu_\alpha + z_\alpha e_0 \varphi) \quad \text{for } \alpha \in \mathcal{I}_K. \quad [11c]$$

The Poisson Eq. 11a determines the electric potential, 11b is the momentum equation, 11c states that the electrochemical potentials of all species are constant in equilibrium. We remark that these equations are not independent, but 11a and 11c together with 10(left) already imply 11b.

Equilibrium surface equations. On the surface Σ between the bulk domains Ω^K , for $K = M, E$, the equilibrium is given by

$$-[(1 + \chi)\varepsilon_0 \nabla \varphi \nu] = q_s \quad [12a]$$

$$[(p\mathbf{1} + (1 + \chi)\varepsilon_0(\nabla \varphi \otimes \nabla \varphi - \frac{1}{2}|\nabla \varphi|^2 \mathbf{1}))\nu] = 0, \quad [12b]$$

$$\mu_\alpha = \mu_\alpha^K \quad \text{for } \alpha \in \mathcal{I}_K, K = E, M. \quad [12c]$$

Specific material models.—Suitable free energy densities for the volume domains Ω^E of the electrolyte, Ω^M of the metal and for the metal-electrolyte surface Σ have been derived in Refs. 16–18 and are summarized here. The free energy densities account for the entropy of mixing and elastic effects due to the finite size of the molecules. For simplicity, we consider only the incompressible limit case. The rather simplistic assumption of constant surface chemical potential of electrons turns out to be just the appropriate way to capture a central feature of metals. It results in the necessary constraint that excess charge is stored on the metal surface.

Not included into the free energy density of the electrolyte are Debye-type electrostatic interactions between ions. As a consequence, the model cannot be expected to reproduce typical square-root behavior in the limit of strong dilution. For the determination of interface capacitance however, the most relevant regime is the opposite limit of concentrated solutions.

Bulk electrolyte material model in Ω^E . The electrolyte in the domain Ω^E is a mixture of several species, one of them being the solvent that we refer to by the index $\alpha = 0$. The index set of the electrolytic species is denoted by \mathcal{I}_E . The mole fractions y_α of the constituents are defined as

$$y_\alpha = \frac{n_\alpha}{n} \quad \text{with } n = \sum_{\beta \in \mathcal{I}_E} n_\beta. \quad [13]$$

In many solvents, ions are solvated, meaning that a number κ_α of solvent molecules are bound into a solvation shell around a center ion. Thus, the partial volume v_α^{ref} of a solvated ion in the electrolyte is typically much larger than the partial volume of the solvent v_0^{ref} . Consequently, we consider the electrolyte as an incompressible liquid mixture of free solvent molecules, undissociated species and solvated ions.^e The incompressibility of the mixture is characterized by the constraint

$$1 = \sum_{\alpha \in \mathcal{I}_E} v_\alpha^E n_\alpha. \quad [14]$$

The chemical potentials for an ideal mixture of solvated ions according to Ref. 17 are in the incompressible limit^f

$$\mu_\alpha = g_\alpha^{ref} + v_\alpha^{ref}(p - p^E) + k_B T \ln(y_\alpha), \quad \alpha \in \mathcal{I}_E, \quad [15]$$

with reference Gibbs free energy $g_\alpha^{ref} = \psi_\alpha^{ref} + v_\alpha^{ref} p^E$, with a constant reference energy ψ_α^{ref} .

Let y_α^E , φ^E and p^E denote the values of the mole fractions, the electric potential and the pressure at some bulk point x^E in Ω^E . In equilibrium, the constant electrochemical potentials according to 11c and the material model 15 then imply for the bulk mole fractions

$$\text{equilibrium: } y_\alpha = y_\alpha^E \cdot \exp\left(-\frac{z_\alpha e_0}{k_B T}(\varphi - \varphi^E) - \frac{v_\alpha^{ref}}{k_B T}(p - p^E)\right) \text{ in } \Omega^E. \quad [16]$$

Note that the pressure p in the electrolytic boundary layer can be expressed as a function of the potential difference $\phi - \varphi^E$ by solving the condition 13 with the representations 16, i.e. the non-linear implicit relation

$$\sum_{\alpha \in \mathcal{I}_E} y_\alpha^E \cdot \exp\left(-\frac{z_\alpha e_0}{k_B T}(\varphi - \varphi^E) - \frac{v_\alpha^{ref}}{k_B T}(p - p^E)\right) - 1 = 0. \quad [17]$$

yields $p = \hat{p}(\varphi - \varphi^E)$.

Bulk metal material model in Ω^M . We consider a metal in the domain Ω^M as a binary mixture of positive metal ions M and free electrons e with $z_e = -1$, i.e. $\mathcal{I}_M = \{M, e\}$. For the metal bulk free energy density, we adopt the Sommerfeld model²² and assume incompressibility, cf.¹⁷ We do not specify the model here, because as a consequence of the following surface material model, it turns out that the metal bulk does not influence any of the results in this paper and therefore can be ignored.

Surface material model on Σ . The surface Σ between the domains Ω^E and Ω^M is considered as mixture of the surface metal ions, surface electrons, electrolytic adsorbates and possibly reaction products of the aforementioned species. The index set of surface constituents is denoted by \mathcal{I}_Σ with $\mathcal{I}_E \cup \mathcal{I}_M \subseteq \mathcal{I}_\Sigma$. Note that we consider on the surface also a solvation effect, whereby each adsorbed ion binds κ_α solvent molecules which propagates into the partial molar area a_α^{ref} .

We adopt the surface free energy model proposed in Ref. 17. In particular, the surface chemical potential of the electrons is assumed to be a constant value depending only on the material and the crystallographic surface orientation. We propose to choose this value related to the electron work function W_Σ of the surface Σ . Analogously to the metal volume, we have an incompressibility constraint on the surface stating $a_M^{ref} n_M = 1$, where a_M^{ref} is the partial area of surface metal ions. On the electrolyte side, we have to account for adsorption from the volume. Since the surface is not necessarily completely covered with adsorbates, we introduce a number density of surface vacancies via

$$n_V = n_M - \sum_{\alpha \in \mathcal{I}_\Sigma \setminus \mathcal{I}_M} \frac{a_\alpha^{ref}}{a_M^{ref}} n_\alpha. \quad [18]$$

^eThis is in contrast to the model of a mixture of undissociated species, the bare center ions and solvent molecules, regardless whether they are free or bound into a solvation shell.

^fIn the classical Poisson-Boltzmann setting, the pressure dependent term $v_\alpha^{ref}(p - p^E)$ is missing. This elastic contribution leads to a limitation of the possible ion concentration. Moreover, the mole fraction y_α also includes ion-solvent interaction.

Then, we define the surface fractions of vacancies and adsorbates by

$$n_s = n_v + \sum_{\alpha \in \mathcal{I}_\Sigma \setminus \mathcal{I}_M} n_\alpha, \quad y_v = \frac{n_v}{n_s} \quad \text{and} \quad (19)$$

$$y_\alpha = \frac{n_\alpha}{n_s} \quad \text{for } \alpha \in \mathcal{I}_\Sigma \setminus \mathcal{I}_M.$$

The chemical potentials of the surface species are

$$\mu_\alpha = \psi_\alpha^{ref} + k_B T \ln(y_\alpha) - \frac{a_\alpha^{ref}}{a_M^{ref}} k_B T \ln(y_v) \quad \text{for } \alpha \in \mathcal{I}_\Sigma \setminus \mathcal{I}_M, \quad (20a)$$

$$\mu_M = \psi_M^{ref} + k_B T \ln(y_v) - a_M^{ref} \gamma, \quad (20b)$$

$$\mu_e = \mu_e^{ref} \quad (=const.). \quad (20c)$$

With respect to the same bulk point in the electrolyte as above, i.e. the values y_α^E , φ^E and p^E , the surface mole fraction of the vacancies, the electrolytic adsorbates, and the surface reaction products, have the representations in terms of the potential difference $U = \varphi|_\Sigma - \varphi^\infty$,

$$y_v = \exp\left(-\frac{a_v^{ref}}{k_B T s} \gamma\right). \quad (21a)$$

$$y_\alpha = y_\alpha^E \exp\left(-\frac{\Delta \tilde{g}_\alpha}{k_B T} - \frac{e_0}{k_B T} z_\alpha U - \frac{a_\alpha^{ref}}{k_B T s} \gamma\right) \quad \text{for } \alpha \in \mathcal{I}_E, \quad (21b)$$

$$y_\beta = \prod_{\alpha \in \mathcal{I}_E} (y_\alpha^E)^{\nu_{\alpha\beta}} \exp\left(-\frac{\Delta \tilde{g}_\beta}{k_B T} - \frac{e_0}{k_B T} \left(\sum_{\delta \in \mathcal{I}_E} \nu_{\delta\beta} z_\delta\right) U - \frac{a_\beta^{ref}}{k_B T s} \gamma\right) \quad \text{for } \beta \in \mathcal{I}_\Sigma \setminus \mathcal{I}_E \setminus \mathcal{I}_M, \quad (21c)$$

where the amount of adsorbates and reaction products on the surface is controlled by the corresponding Gibbs energies defined by

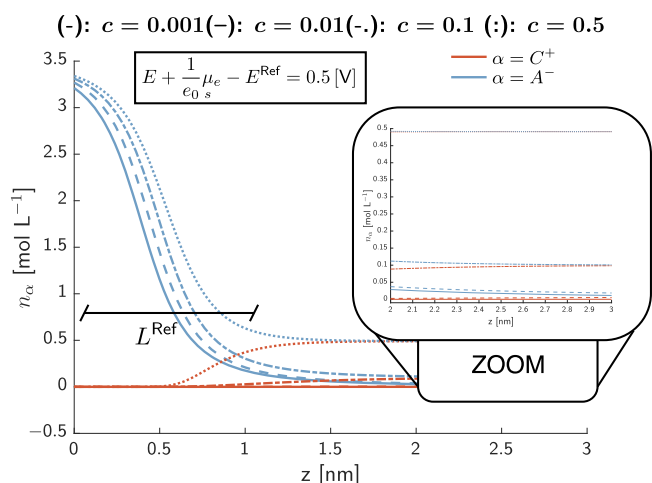


Figure 5. Numerical computation of the space charge layer in front of a single crystal metal surface at an applied voltage of $E + \frac{1}{e_0} \mu_e - E^{ref} = 0.5V$ for various bulk concentrations c .

$$\Delta \tilde{g}_\alpha = \psi_\alpha^{ref} - (\psi_\alpha^E + v_\alpha^{ref} p^E) \quad \text{for } \alpha \in \mathcal{I}_E, \quad (22a)$$

$$\Delta \tilde{g}_\beta = \psi_\beta^{ref} - \sum_{\alpha \in \mathcal{I}_M} \nu_{\alpha\beta} (\mu_\alpha^M + e_0 z_\alpha U^M) - \sum_{\alpha \in \mathcal{I}_E} \nu_{\alpha\beta} (\psi_\alpha^E + v_\alpha^{ref} p^E) \quad \text{for } \alpha \in \mathcal{I}_E. \quad (22b)$$

The above representations and the definition 19 of the surface mole fractions yield an algebraic equation which determines the surface tension γ as a function of U .

Model Application for Solid Electrode Surfaces

It is well known that at the surface Σ between a metal and an electrolyte a charged double layer exists, which decays into the electrolyte bulk electrolyte. For Poisson–Boltzmann and Gouy–Chapman type models the space charge layer width is in the order of the Debye length

$$L^{Debye} = \sqrt{\frac{(1 + \chi) \epsilon_0 k_B T}{e_0^2 c}}, \quad (23)$$

where c is the bulk salt concentration. However, for the incompressible mixture model of Section 3.2, which incorporates solvation effect of the ionic species, we find that the space charge layer width is in the order of $L^{ref} = 1[\text{nm}]$, almost independent of the bulk concentration c , however, dependent on the applied voltage. Figure 5 displays the computed space charge layer, i.e. the cation and anion densities n_α as function of the electrode distance z for an applied voltage of $E + \frac{1}{e_0} \mu_e - E^{ref} = 0.5 \text{ V}$.

If the dimension of the considered experimental setup is considerably larger than $1[\text{nm}]$, say in the range of several μm , it often is reasonable to consider the surface Σ as an infinite planar surface and the electrolyte domain Ω^E as a half space. We chose the coordinates (x, y, z) such that Σ corresponds to the plane $z = 0$. Since we are only interested in the boundary layer, we can choose a sufficiently large z^E and approximate the electrolyte domain as $\Omega^E = \Sigma \times [0, z^E]$.

Planar single crystal surface.—Given the simple geometric setting and assuming the surface to be homogeneous in space, all quantities in the electrolyte can only depend on the spatial coordinate normal to Σ . Then, we define the boundary layer- and the surface charge density by

$$Q^{BL} = \int_0^{z^E} q \, dz = -e_0 \sum_{\alpha \in \mathcal{I}_\Sigma \setminus \mathcal{I}_M} z_\alpha n_\alpha. \quad (24)$$

In equilibrium, both quantities are completely determined by the potential difference $U = \varphi - \varphi^E$. It is a remarkable feature of the applied material model in Section 3.2 that it is possible to determine the boundary layer charge density Q^{BL} as function of U^E without needing to spatially resolve the bulk Eqs. 11–12, i.e.

$$Q^{BL} = \text{sgn}(U) \sqrt{2\epsilon_0(1 + \chi)(\hat{p}(U) - p^E)} =: \hat{Q}^{BL}(U). \quad (25)$$

where $\hat{p}(U)$ is the material pressure determined from 17. Moreover, all surface mole fractions are determined according to 21 and we get for the surface charge density

[§]The typeface \hat{Q} indicates that this is a function $U = \varphi - \varphi^E$ and not the applied voltage E .

$$\hat{Q}_s(U) = \frac{\sum_{(\alpha \in \mathcal{I}_E)} z_\alpha e_0 y_\alpha + \sum_{(\alpha \in \mathcal{I}_E)} \sum_{(\beta \in \mathcal{I}_\Sigma \setminus \mathcal{I}_{E,M})} \nu_{\alpha\beta} z_\alpha e_0 y_\beta}{a_V^{ref} y_V + \sum_{(\alpha \in \mathcal{I}_\Sigma \setminus \mathcal{I}_M)} a_\alpha^{ref} y_\alpha}. \quad [26]$$

Thus, we can introduce the differential capacity as

$$\hat{C}(U) = \frac{d}{dU} (Q^{BL}(U) + Q(U)) = C^{BL}(U) + C(U) \quad [27]$$

Under the standard assumption that the potential difference between an ideally non-polarizable reference electrode and the bulk electrolyte remains constant under potential variations, it is possible to show¹⁷ that

$$U = \varphi - \varphi^E = E + \frac{1}{e_0 s} \mu_e - E^{ref} \quad \text{with} \quad E^{ref} = \text{const.}, \quad [28]$$

where E is the applied voltage in a three electrode setup, μ_e the surface chemical potential of electrons, and E^{ref} a constant¹⁷ which depends on the actual reference electrode. For a specific surface Σ , the differential capacity in the absolute scale E is given by an appropriate shift of 27, i.e.

$$C(E) = \hat{C}\left(E + \frac{1}{e_0 s} \mu_e - E^{ref}\right). \quad [29]$$

Modeling of planar polycrystal surfaces.—We consider now a planar surface Σ which is composed of N facets Σ_i , i.e. $\Sigma = \bigcup_{i=1}^N \Sigma_i$ as sketched in Fig. 2. We assume finite size surfaces patterns that can be periodically extended to the whole plane. We denote by $|\Sigma_i|$ the area of the facet Σ_i whereby the total area of Σ is $|\Sigma| = \sum_{i=1}^N |\Sigma_i|$ and surface fraction $s_i := \frac{|\Sigma_i|}{|\Sigma|}$. We make the assumption

The facet boundaries $\partial\Sigma_i \cap \partial\Sigma_j$ for $i \neq j$ constitute no independent thermodynamic entities.

Thus, each facet Σ_i can be treated as a finite size planar single crystal surface, and we can apply the material model of Section 3.2 on each facet Σ_i separately. Since the surface density of metal ions depends on the crystallographic orientation of the surface, the material parameter a_M is different for each individual facet Σ_i . As a consequence, in the absence of adsorption to the surface, the surface tension γ differs between the facets Σ_i .^h In addition, we have to assign to each facet Σ_i a constant value of μ_e , which has to be related to the electron work function on a surface of the respective crystallographic orientation. Because all facets are connected by electric conductors, the electrochemical potential of the electrons is constant over all grains in the metal Ω_M , i.e.

$$(\mu_e - e_0 \varphi)|_{\Sigma_i} = (\mu_e - e_0 \varphi)|_{\Omega_M} = (\mu_e - e_0 \varphi)|_{\Sigma_j}. \quad [30]$$

Between each two surfaces, we thus have the pairwise potential difference

$$\varphi|_{\Sigma_j} - \varphi|_{\Sigma_i} = \frac{1}{e_0 s} (\mu_e|_{\Sigma_j} - \mu_e|_{\Sigma_i}). \quad [31]$$

Patterned planar surface. As in the single crystal case before, we can expect boundary layers that decay exponentially from the surface Σ into the electrolyte bulk. The length scale of the boundary layer is given by the Debye length according to 23 and the electrolyte bulk can be characterized by certain constant far field values y_α^E , φ^E and p^E in a distance from the surface that is large compared to 1 [nm].

^hOne has to be careful with an interpretation of this fact. Surface tension of planar solid surfaces is difficult to measure and one has to distinguish between the “thermodynamic” surface tension and the “interfacial tension”, cf.¹⁸

We assume that the electrolyte in Ω^E is not influenced by any other boundary layer than the one at Σ . Given the applied potential $E - E^{ref}$ we set $\varphi^E = 0$, which corresponds to an ideally polarizable reference electrode. Then, the state in the electrolyte in Ω^E is given by the the generalized Poisson-Boltzmann boundary value problem similar to Refs. 16, 17, 19

$$-(1 + \chi)\varepsilon_0 \Delta\varphi = q(\varphi, p) \quad \text{in } \Omega^E, \quad [32a]$$

$$1 = \sum_{\alpha \in \mathcal{I}_E} y_\alpha(\varphi, p) \quad \text{in } \Omega^E, \quad [32b]$$

$$\varphi|_{\Sigma_i} = \frac{1}{e_0 s} (\mu_e|_{\Sigma_i} - (E - E^{ref})) \quad \text{on } \Sigma, \quad [32c]$$

$$\nabla\varphi \rightarrow 0 \quad \text{far away from } \Sigma, \quad [32d]$$

where $y_\alpha(\varphi, p)$ is given by 16 for $\alpha \in \mathcal{I}_E$.

Given a solution of 32 in Ω^E , the boundary layer charge q is determined by y_α according to 7 and 14. The surface charge density can be calculated by 26 on each facet Σ_i separately and we get

$$Q_{\Sigma_i} = \hat{Q}_s\left(E - E^{ref} + \frac{1}{e_0 s} \mu_e|_{\Sigma_i}\right) \quad [33]$$

Thus for the surface Σ , we conclude

$$Q_s^{\text{poly}}(E) = \sum_{i=1}^N s_i \hat{Q}_s\left(E - E^{ref} + \frac{1}{e_0 s} \mu_e|_{\Sigma_i}\right). \quad [34]$$

Upon solution of the boundary value problem, the boundary layer charge density is computed from

$$Q_{\text{poly}}^{\text{BL}}(E) = -\frac{1}{|\Sigma|} \int_{\Omega^E} q(x) dx, \quad [35]$$

Finally, the total surface charge is $Q_{\text{poly}}(E) = Q_{\text{poly}}^{\text{BL}}(E) + Q_{\text{poly}}(E)$ and the differential capacity of the patterned surface is computed by taking the derivative with respect to the applied potential E .

Ensemble of planar single crystal surfaces. The total boundary layer charge density can be decomposed into the contributions adjacent to the different facets Σ_i , viz.

$$Q^{\text{BL}} = \sum_{i=1}^N s_i Q_{\Sigma_i}^{\text{BL}} \quad \text{with} \quad Q_{\Sigma_i}^{\text{BL}} = -\frac{1}{|\Sigma_i|} \int_{\Sigma_i \times [0, \infty)} q(z) dz. \quad [36]$$

Since boundary effects propagate into the interior with a length scale in the order of the chosen reference length of the electrolyte, boundary effects due to the finite size of Σ_i can be neglected once the characteristic facet diameter is sufficiently large, i.e. 1 [nm] $\ll d^{\text{facet}}$. Then, the charge density in front of Σ_i is well approximated by the boundary layer charge 25 at a planar single crystal with the same material parameters as Σ_i , i.e.

$$Q_{\Sigma_i}^{\text{BL}} - \hat{Q}^{\text{BL}}\left(E - E^{ref} + \frac{1}{e_0 s} \mu_e|_{\Sigma_i}\right) \rightarrow 0 \quad \text{for} \quad \frac{1[\text{nm}]}{d^{\text{facet}}} \rightarrow 0. \quad [37]$$

Thus, in the limit of large facets, the boundary layer charge density $Q_{\text{poly}}^{\text{BL}}$ of the polycrystal is given by the according density of an ensemble of non-interacting (infinitely large) planar single crystal surfaces, all in contact with the same electrolyte, viz.

$$Q_{\text{poly}}^{\text{BL}}(E) = \sum_{i=1}^N s_i \hat{Q}^{\text{BL}}\left(E - E^{ref} + \frac{1}{e_0 s} \mu_e|_{\Sigma_i}\right), \quad [38]$$

The boundary layer capacity related to 38 is given by 3. As 33 can be applied independent of the size of d^{facet} , we conclude

$$C_{\text{poly}}(E) = \sum_{i=1}^N s_i \hat{C} \left(E - E^{\text{ref}} + \frac{1}{e_0} \mu_e |_{\Sigma_i} \right). \quad [39]$$

The potential of zero charge E^{PZC} is determined from Eq. 37, i.e. $Q_{\text{poly}}^{\text{BL}}(E) \stackrel{\text{!}}{=} 0$. Intuitively one would expect that the potential of zero charge E^{PZC} is determined as $\frac{1}{e_0} \sum_{i=1}^N s_i \mu_e |_{\Sigma_i} + E^{\text{ref}}$. But since the functions \hat{C}^{BL} are non-linear with respect to their argument, this does not hold, i.e. in general

$$E^{\text{PZC}} - E^{\text{ref}} \neq \frac{1}{e_0} \sum_{i=1}^N s_i \mu_e |_{\Sigma_i} =: \bar{\mu}_e \quad [40]$$

but

$$Q_{\text{poly}}^{\text{BL}}(E)|_{E=E^{\text{PZC}}} = 0. \quad [41]$$

In Section 6 we provide some exemplary calculations showing the difference between $E^{\text{PZC}} - E^{\text{ref}}$ and $\bar{\mu}_e$ for several parameter variations.

Surfaces of Finite Size Pattern and Approached Limit Relations

Given a polycrystalline surface with a finite size pattern of facets and their individual surface potentials, one has to expect that the capacitance can only be determined numerically from a spatially resolved FEM solution in Ω^{E} and that this solution depends on the specific geometry of the facets. In this section, we study numerically the capacitance for certain examples of surface patterns. We assume that the electrolyte consists of the solvent, denoted by S , and the anions A and cations C of a completely dissociated salt, i.e. $\mathcal{T}_{\text{E}} = \{A, C, S\}$. For the numerical simulations we solve 35 with physical constants and material parameters as given in Table I. We chose the reference number density according to pure water. Since we apply the simplified model of a constant dielectric susceptibility, we chose a value for χ that refers to a strongly concentrated solution and thus is considerably lower than $\chi_{\text{H}_2\text{O}} = 80$, cf. e.g.²³

In order to keep the focus of this section sharp, we assume here that the electrolyte is non-adsorbing. If in addition also adsorption has to be taken into account, surface charge and surface capacity can be computed in purely algebraic manner by a post-processing step applying 34 and its derivative with respect to the applied potential, respectively.

Pattern of two equally sized facets.—We consider first the most simple configuration of a symmetric bi-crystalline surface, where $N = 2$, $s_1 = s_2 = 1/2$. We choose an average potential $\bar{\mu}_e$ such that $\mu_e |_{\Sigma_1} - \bar{\mu}_e = -(\mu_e |_{\Sigma_2} - \bar{\mu}_e) = -0.1 \text{ eV}$. On the surface, we

Table I. Physical constants and parameters used in the numerical simulations.

dielectric constant	$\epsilon_0 = 8.854\,187\,817\,62 \times 10^{-12} \text{ C (Vm}^{-1}\text{)}$
Boltzmann constant	$k_B = 1.3806488 \times 10^{-23} \text{ J K}^{-1}$
elementary charge	$e_0 = 1.602\,176\,565 \times 10^{-19} \text{ C}$
Avogadro number	$N_A = 6.02214129 \times 10^{23} \text{ mol}^{-1}$
temperature	$T = 298.15 \text{ K}$
reference pressure	$p^{\text{ref}} = 1 \times 10^5 \text{ Pa}$
dielectric susceptibility	$\chi = 15$
charge number	$-z_A = z_C = 1, z_S = 0$
solvation number	$\kappa_\alpha = 10$
reference number density	$n^{\text{ref}} = \frac{1}{v_0^{\text{ref}}} = 55.5 \text{ mol l}^{-1}$
bulk salt concentration	$c^{\text{E}} [\text{mol l}^{-1}]$
specific volumes	$v_\alpha^{\text{ref}} = (1 + \kappa_\alpha) v_0^{\text{ref}}$

thus have the boundary values $\varphi|_{\Sigma_i} = \Phi_i$ for $i = 1, 2$ with $\Phi_1 = -\Phi_2 = -0.1 \text{ V}$. The simplest realization of this configuration consists of a pattern of parallel stripes with alternating prescribed potential. Here, we let d^{facet} denote the width of the stripes. With an appropriate choice of the coordinate system, the boundary values can be described by a 1D-function such that

$$\varphi(x) = \begin{cases} \Phi_1 & \text{for } 2|x| < d^{\text{facet}}, \\ \Phi_2 & \text{for } 2|x - d^{\text{facet}}| < d^{\text{facet}}, \end{cases} \quad [42]$$

and periodic continuation. Accordingly, the potential and the charge density in the electrolyte domain $z > 0$ can be determined from a 2D-FEM computation by integration of the free charge q in space according to 35. The choice of the boundary values implies that in the far field the potential approaches $\varphi \rightarrow \varphi^{\text{E}} = -(E - E^{\text{ref}}) - \frac{1}{e_0} \bar{\mu}_e$. Plots of the electric potential for $E = E^{\text{ref}} - \frac{1}{e_0} \bar{\mu}_e$ and an electrolyte with a bulk

concentration of 0.1 mol l^{-1} and the remaining parameters according to Table I are given in Fig. 6 (left). In the upper plot, where the facet size was chosen as $d^{\text{facet}} = 10L^{\text{Debye}} \approx 12.28 \text{ nm}$, one can observe that the piece-wise constant boundary data to a large extent propagates into the electrolyte and decays with increasing distance to the boundary. To the contrary, in the lower plot, where $d^{\text{facet}} = \frac{5}{2}L^{\text{Debye}} \approx 3.07 \text{ nm}$, the profile of the potential is dominated by facet boundary effects such that the regions of parallel iso-lines almost disappear.

Next, the applied potential is varied in positive and in negative direction and the boundary value problem 32 is solved. From this solution, the free charge density q and $Q^{\text{BL}}(E)$ are computed. Figure 6 (right) shows the resulting capacity for different electrolyte concentrations in dependence of the facet size d^{facet} . We observe for increasing facet size d^{facet} a convergence of the computed capacity curves to the algebraic solution 3. In particular, in the potential range outside of the lowest and the largest position of the maxima, the algebraic expression 3 is always a good characterization of the polycrystalline surface, independent of the facet size. Figure 6 also shows that the convergence depends on the electrolyte bulk concentration. We thus repeat the numerical experiment over a larger range of parameter variation, such that the bulk concentration is varied between $10^{-4} \text{ mol l}^{-1}$ and 1 mol l^{-1} and the facet diameter is changed between 0.2 nm and 120 nm . We observe in Fig. 7 that while the behavior with respect to the bulk concentration is not monotonous, in any case the approximation error of 3 in the maximum norm can be bounded by some term proportional to the inverse of d^{facet} .

In addition, 3D-FEM simulations with a checkerboard pattern of the surface were performed where the boundary values are given by periodic continuation of

$$\varphi(x, y) = \begin{cases} \Phi_1 & \text{for } \max(|x|, |y|) < d^{\text{facet}}, \quad \text{sgn}(x y) > 0, \\ \Phi_2 & \text{for } \max(|x|, |y|) < d^{\text{facet}}, \quad \text{sgn}(x y) < 0. \end{cases} \quad [43]$$

The observations from the 3D computations are analogous as for the 2D case. Since for given d^{facet} , the length of the contact lines in the checkerboard pattern is double compared to the striped pattern represented by the 2D case, convergence for increasing facet size is a bit slower here. Together, the 2D and the 3D results indicate that the shape of the facets is not relevant as long as the facet diameter d^{facet} is sufficiently large compared to a reference length in the order of $1 [\text{nm}]$. We conclude that already the covered surface fraction of the facets and the corresponding single crystal capacities fully determine the capacity of a polycrystalline surface of sufficiently large facet size.

As FEM simulations in 3D are computationally expensive, we used anisotropic grids with a mesh grading with respect to the a-priori known structure of the potential, see Fig. 8. To check that the grid is sufficiently fine, we compared the resulting capacity curves from numerical solutions of the boundary value problem 32 on

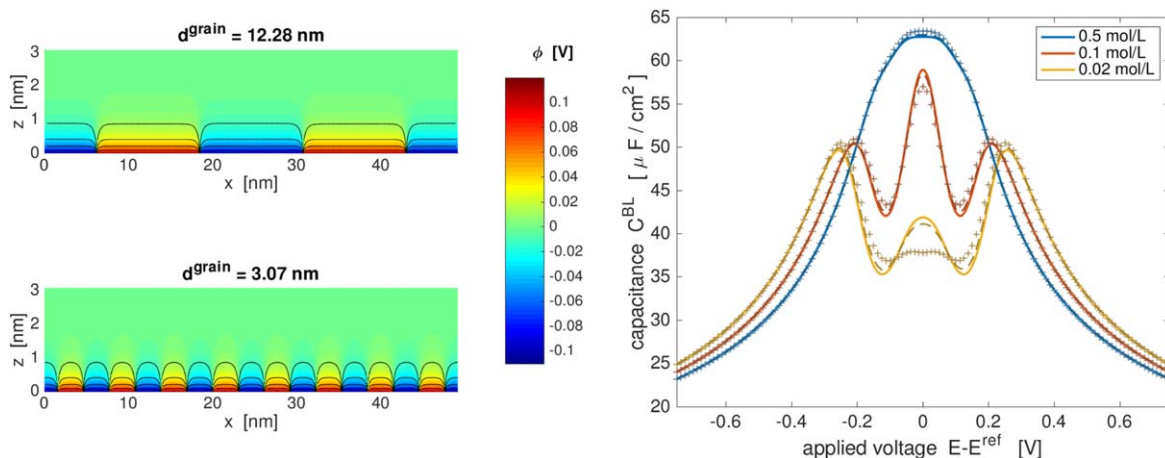


Figure 6. Left: profile of the electric potential for different diameters of the surface stripes. Right: capacity curves for different electrolyte concentrations, where solid lines (—) refer to the algebraic solution according to 3, FEM solution for facet size $d^{\text{facet}} = 3.07$ nm is indicated by markers (+), and for $d^{\text{facet}} = 12.28$ nm by dashed lines (- -).

different refinement levels of the initial mesh. Refined meshes on the refinement levels 3, 4 and 5 consisted of 2 601, 18 513 and 139 425 nodes, respectively. Figure 8 shows the convergence of the computed capacity curves when refining the mesh.

Characterization of PZC and limiting behavior.—In the previous section, we did not discuss the PZC for the patterned polycrystalline surface. The reason is that due to the symmetry, i.e. $s_1 = s_2$, it always coincides with the chosen reference potential. In order to introduce some asymmetry, we slightly modify the configuration to $N=2$, $s_1 = 1/3$, $s_2 = 2/3$, and again set $\Phi_1 = -\Phi_2 = -0.1$ V. For a 2D-FEM simulation of this configuration, we choose

$$\varphi_s(x) = \begin{cases} \Phi_1 & \text{for } 2|x| < d^{\text{facet}}, \\ \Phi_2 & \text{for } |x - \frac{3}{2}d^{\text{facet}}| < d^{\text{facet}}, \end{cases} \quad [44]$$

with periodic continuation of the boundary data. As in the previous example, we again observe that the capacity of the patterned surface approaches 3 for large facet sizes d^{facet} , see Fig. 9 (left). From the computed boundary charge as a function of the applied potential

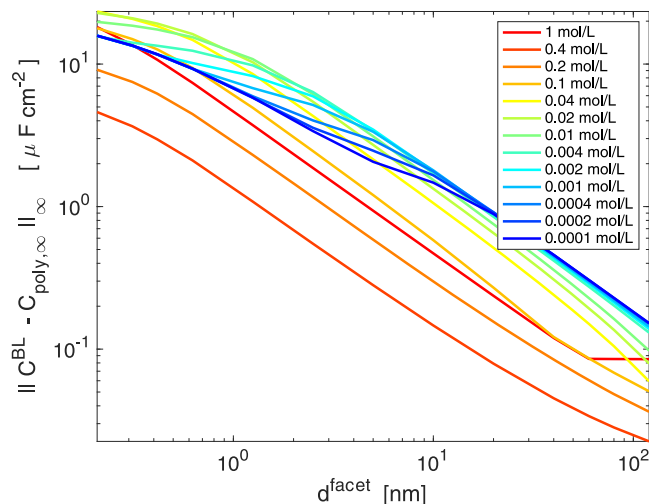


Figure 7. Approximation error of 3 over the characteristic diameter d^{facet} of the facets for the symmetric bi-crystal and various electrolyte concentrations.

according to 35, we can now determine the potential of zero charge of the patterned surface with finite d^{facet} . We observe that for a fixed facet size d^{facet} , the PZC is not constant but increases with the bulk electrolyte solution, cf. Fig. 9 (right). Moreover, the potential range, in which the PZC varies with respect to the bulk concentration, gets wider for increasing d^{facet} . As a limit for $d^{\text{facet}} \rightarrow \infty$, the PZC reaches the values we get from the surface fraction weighted averaging of single crystals according to 3. Since the capacity of a planar single crystal is approximately quadratic at its PZC, the boundary layer charge behaves almost cubic. Thus, one should not expect, that the linear combination of single crystal capacities would attain its PZC at the respective linear combination of the individual PZCs.

In addition, another limit is of interest, however more from a theoretical point of view. Let us consider $d^{\text{facet}} \rightarrow 0$, although a pattern at the atomic length scale or even blow that scale cannot be realized in practice. We observe, that for $d^{\text{facet}} \rightarrow 0$, the capacity curve changes from the three-maxima shape according to 3 into the typical two-maxima or camel shape that is well known from the planar single crystal. In fact, for $d^{\text{facet}} \rightarrow 0$, the capacity converges to the capacity of a planar single crystal surface where the PZC is determined as the sum of the PZCs on the contributing facets weighted by their respective surface fraction s_i according to 5. Moreover, this limit of the PZC is independent of the bulk electrolyte concentration.

Surface roughness.—Because of surface roughness, the *actual surface area* of real surfaces is larger compared to their ideally plain counterparts which are characterized by their so called *visible surface area*. As a measure of this effect, the surface roughness factor W is introduced as the quotient of the real surface area over the visible. Surface roughness appears on a large range of different length scales, from “physical inhomogeneity” on the atomic length scale to “geometric roughness” on a macroscopic scale of several μm . A lot of attention was devoted to the analysis of “geometric” surface roughness which in experiments may be caused e.g. by electrode pre-treatment like polishing. In the context of electrochemical impedance analysis, roughness is then often analyzed in the framework of fractal geometry, where on the larger scales, an interaction of the boundary layer with bulk transport properties of electrolyte has to be expected.

We want to concentrate on the effect of surface roughness on the boundary layer capacitance and therefore consider only deformations of an ideally plain surface that are on a length scale of the facet size d^{facet} . We return to the setting of the symmetric bi-crystal of Section 5.1 and let the surface be given by

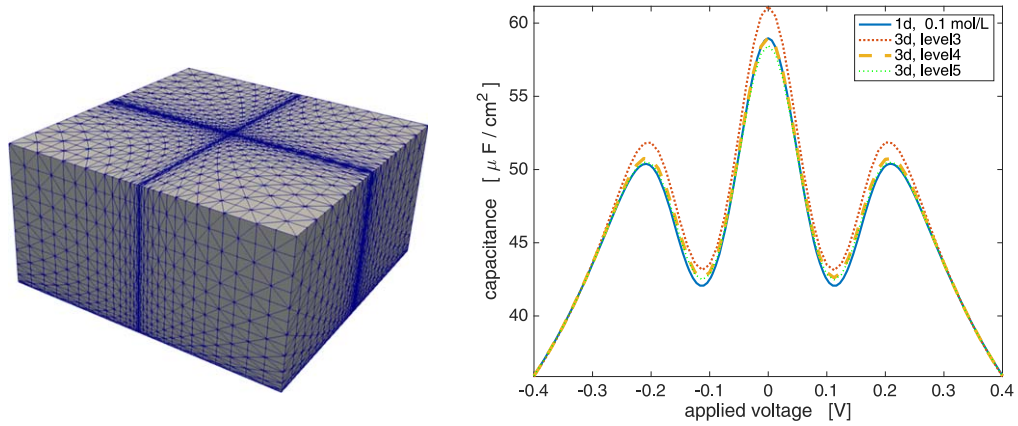


Figure 8. Left: numerical grid on refinement level 3, as used for computation in Fig. 2. Right: computed capacity curves for different levels of grid refinement.

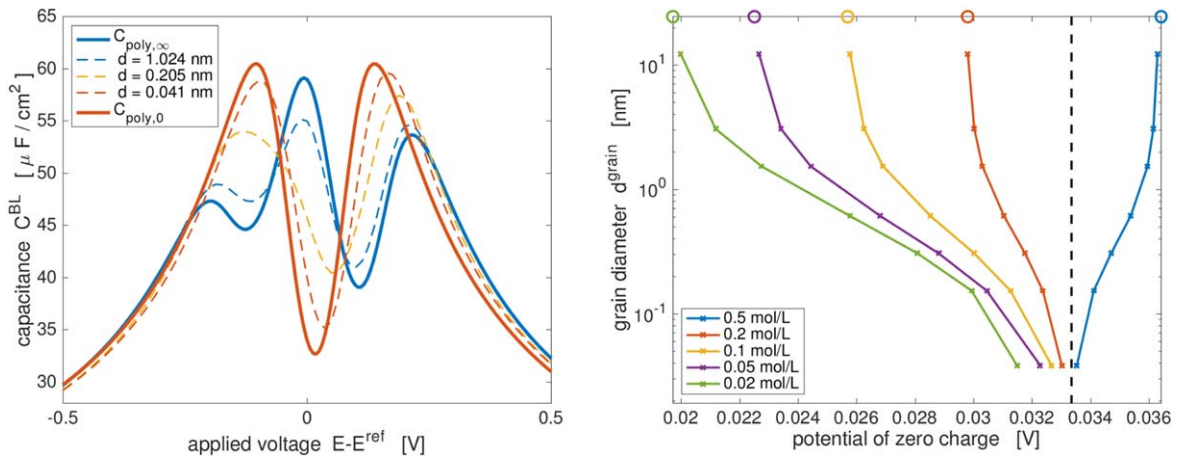


Figure 9. Left: capacity curves for 0.1 mol L⁻¹ electrolyte and different facet size parameters (dashed lines - -). Limits for large facet diameter (blue, solid —) and vanishing facet diameter (red, solid —). Right: lines show the position of the PZC of the patterned surface in dependence of the facet size d^{facet} for different bulk concentrations. The circles on the to indicate the values of $E_{\text{poly}}^{\text{PZC}}$ according to 3 that are approached for $d^{\text{facet}} \rightarrow \infty$ and the dashed line refers to $E_{\text{poly}}^{\text{PZC}}$ according to 5.

$$\frac{d^{\text{facet}}}{h^{\text{max}}} h(x) = \begin{cases} x & \text{for } 2|x| < d^{\text{facet}}, \\ (d^{\text{facet}} - x) & \text{for } 2|x - d^{\text{facet}}| < d^{\text{facet}}, \end{cases} \quad [45]$$

where the parameter h^{max} is the maximal elevation of the surface over the supporting pane, see Fig. 10. This results in a surface roughness factor of

$$W = \frac{\sqrt{(d^{\text{facet}})^2 + (h^{\text{max}})^2}}{d^{\text{facet}}}. \quad [46]$$

We performed 2d FEM simulations of the boundary layer in dependence of the applied potential and the electrolyte concentration varying the surface roughness parameter relative to the Debye length as $h^{\text{max}}/L^{\text{Debye}} = \frac{5}{8}, \frac{5}{4}, \frac{5}{2}$. The respective surface roughness factors according to 46 are $W = 1.002, 1.0078, 1.031$. We observe that with increasing h^{max} , the capacity curves deviate stronger from the calculated capacity of the perfectly smooth surface, see Fig. 11 left. Moreover, Fig. 11 right indicates that surface roughness can be very accurately taken into account by multiplying the surface roughness factor W to the capacity of the perfectly plain surface, i.e.

$$C(E) = W(h^{\text{max}}) C_{\text{poly}}^{\text{BL}}(E). \quad [47]$$

Discussion of the Idealized Polycrystal

Within this discussion, we always apply the limit of large facet size $1 \text{ [nm]} \ll d^{\text{facet}}$ related to 3, keeping in mind, that this limit is already well approached for $d^{\text{facet}} = 20 \text{ nm}$.

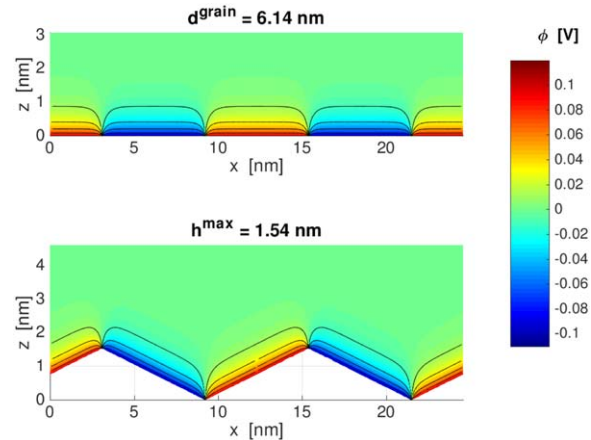


Figure 10. Electric potential for an electrolyte of 0.1 mol L⁻¹ salt concentration in contact with a symmetric bi-crystal surface at the applied potential $E = E^{\text{ref}} - \frac{1}{e_0} \mu_e$. Top: flat surface, i.e. $h^{\text{max}} = 0$, bottom: differently oriented facets with $h^{\text{max}} = 1.54 \text{ nm}$.

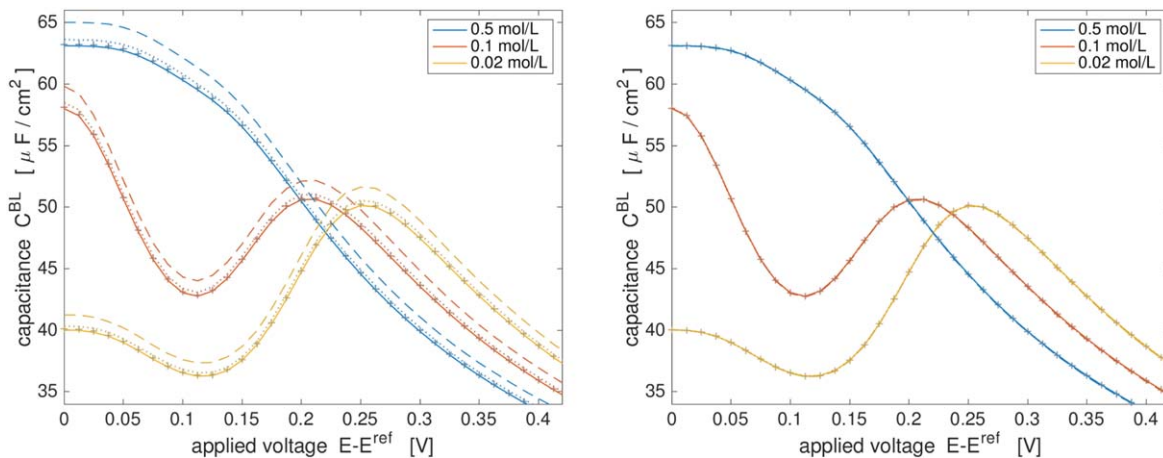


Figure 11. Left: detail of the boundary layer capacity for different electrolyte concentrations and surface roughness with $h^{\max} = 0.38$ nm (markers +), $h^{\max} = 0.77$ nm (···) and $h^{\max} = 1.54$ nm (- -). Right: correction by surface roughness factor according to 46.

Difference of PZC.—In the previous section, we kept the potential difference between the two considered facets constant (viz. 0.2 V). However, this difference is a material dependent characteristic quantity that varies between different materials or different crystallographic orientations. While differences of the PZC, respective μ_e , between differently oriented surfaces are considered minor for some metals, e.g. “low melting metals” like Cd, Sn, Pb, Zn and Bi, cf.,^{5,10} considerable differences between the low index facets are reported for e.g. Ag, Au, Cu, Pt and W, cf.²⁴ Thus, we examine the situation of an bi-crystal with equal surface fractions $s_1 = s_2 = 1/2$ and vary the difference of the surface chemical potential of the electrons $\Delta\mu_e = \mu_e|_{\Sigma_1} - \mu_e|_{\Sigma_2}$ between 0 eV and 0.8 eV. This corresponds to varying the boundary values such that $0V \leq \Phi_1 - \Phi_2 \leq 0.8V$. We observe, that for $\Phi_1 - \Phi_2 < 0.115V$ the capacity retains the typical camel shape. For $0.115V < \Phi_1 - \Phi_2 < 0.375V$ there is a three maximum shape, whereas for larger potential differences between the facets, we have a four-maximum configuration that again allows to identify the two local extrema of the individual facets, see Fig. 12. Once more, we stress that in experiments one should be aware of the fact that for a polycrystalline surface the PZC in general is not found at a local capacity minimum! For a sufficiently large potential difference $\Phi_1 - \Phi_2$, the PZC is in general found between the inner two local maxima of the capacity, and only for specific configurations of the surface fractions s_i the PZC is located at a local capacity minimum. Even more, for moderate $\Phi_1 - \Phi_2$, the PZC is located near a local capacity maximum!

As stated in Section 4.2, the potential of zero charge

$$E^{\text{PZC}} - E^{\text{ref}} \neq \bar{\mu}_e \quad [48]$$

but, it has to be determined from a solution of the non-linear equation $Q_{\text{poly}}^{\text{BL}}(E) = 0$. This solution is dependent on the salt concentration c , the the surface fractions s_i , and the $\mu_e|_{\Sigma_i}$. For a bi-crystal, Fig. 13 displays the difference $\bar{\mu}_e - (E^{\text{PZC}} - E^{\text{ref}})$.

Adsorption to the surface.—To study the effect of adsorption, we return to the simple configuration of a symmetric bi-crystal in Section 5.1, i.e. we choose $N = 2$, $s_1 = s_2 = 1/2$. We assume that the adsorption energies Δg_α do not differ between the different facets. In particular, by the choice of

$$\Delta g_A = -0.25 \text{ eV}, \quad \Delta g_C = +1 \text{ eV}, \quad \Delta g_S = -0.0735 \text{ eV}. \quad [49]$$

we assume, that cations effectively do not adsorb while anions and the solvent are allowed to adsorb to the surface. For simplicity and

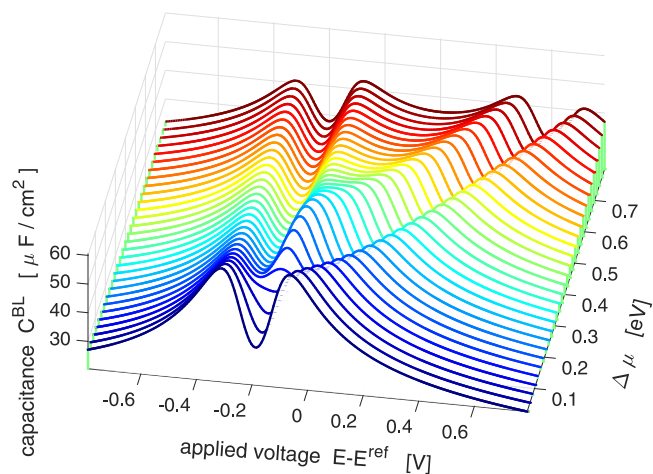


Figure 12. Capacity curves for varying difference $\Delta\mu_e = \mu_e|_{\Sigma_1} - \mu_e|_{\Sigma_2}$ for a bi-crystal with equal surface fractions $s_1 = s_2$.

(-): $c = 0.001$ (·): $c = 0.01$ (:): $c = 0.1$

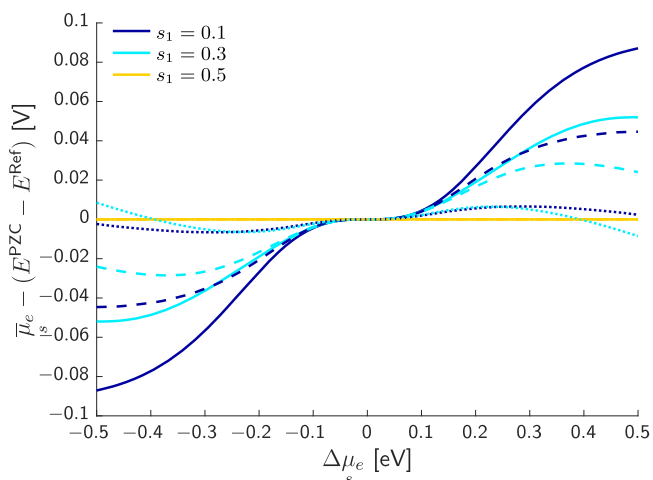


Figure 13. Numerical computation of the difference between the potential of zero charge E^{PZC} and the average surface chemical potential of electrons $\bar{\mu}_e$ for a bi-crystal as function of $\Delta\mu_e = \mu_e|_{\Sigma_1} - \mu_e|_{\Sigma_2}$ for various surface fractions s_1 ($s_2 = 1 - s_1$) and electrolyte concentrations c .

clarity of presentation, we do not consider surface reactions like solvation shell stripping or electron transfer reactions. An extension is straightforward by applying 21c for the reaction products and 26 for the surface charge. In the numerical computation, we use for the radius and the partial area of the adsorbed species

$$r_{\alpha}^{ref} = \left(\frac{3}{4\pi} \psi_{\alpha}^{ref} \right)^{\frac{1}{3}}, \quad a_{\alpha}^{ref} = \frac{8}{\sqrt{3}} \pi (r_{\alpha}^{ref})^2. \quad [50]$$

According to 34, the surface capacity of a patterned surface only depends on the material parameters of the contributing facets and their surface fractions s_i , but not on the facet geometry or the facet size parameter d^{facet} . Thus, we can combine 3 and 34 to conclude that for large facet size, the capacity of a perfectly plain polycrystal surface is

$$C_{\text{poly}} = \sum_{i=1}^N s_i \hat{C} \left(E - E^{ref} + \frac{1}{e_0} \mu_{e|\Sigma_i} \right). \quad [51]$$

Figure 14 shows the capacity curves of a single crystal surface and illustrates the construction for a bi-crystal according to 51. As already known for single crystal surfaces, if there is adsorption from the electrolyte, the PZC depends on the electrolyte and its bulk concentration, cf. e.g.¹⁷ The same also holds true for the polycrystal and we conclude from 3 and 34 that¹ for $l[\text{nm}] < d^{\text{facet}} \rightarrow \infty$, the determination of $E_{\text{poly}}^{\text{PZC}}$ requires the solution of the non-linear algebraic equation

$$0 = \sum_{i=1}^N s_i \hat{Q} \left(E_{\text{poly}}^{\text{PZC}} - E^{ref} + \frac{1}{e_0} \mu_{e|\Sigma_i} \right). \quad [52]$$

Multiple different facets.—The above results can easily be extended to more complex polycrystalline surfaces with many facets of different type. We consider the case of $N=4$ different types of facets $\Sigma_1, \Sigma_2, \Sigma_3, \Sigma_4$ with the respective surface fractions $s_1 = 4/9, s_2 = s_3 = 2/9, s_4 = 1/9$. Also, we want to have junction points where more than two different facets meet. One possible simple realization on a 2D surface is the periodic symmetric continuation of the pattern sketched in Fig. 15. The boundary data is given as $\varphi = \Phi_i$ on Σ_i , for $i = 1, 2, 3, 4$. We choose $\Phi_1 = -\Phi_2 = -0.1$ V. First, we let $\Phi_4 = \Phi_1$ and $\Phi_3 = \Phi_2$ and get slightly non-symmetric capacity curves¹, see Fig. 15. Next, we change Σ_3 such that $\Phi_3 = -0.061$ V while still $\Phi_4 = \Phi_1$. Finally, set $\Phi_4 = .085$ V and keep the remaining boundary values as before, see Fig. 15 bottom line.

As in Section 5.1, we checked convergence of the capacity calculated from 3D-FEM simulation for finite facet size d^{facet} to the limit Eq. 3 for $d^{\text{facet}} \rightarrow \infty$ and grid convergence of the numerical solutions.

Stochastic distribution of surface patterns.—A precise measurement of all surface facets and their corresponding work functions is extremely expensive, if possible, and even measurements on very similar facets may contain some scatter. Hence, the input values for the mathematical model of the foregoing section can only be determined to a certain precision, which has to be taken into account when realistic polycrystalline surfaces are to be described. We sketch therefore a stochastic description of the polycrystalline surface based on the derived deterministic model and provide some numerical examples of the double layer capacity.

Consider a surface Σ of $N > 1$ facets Σ_i . We define the set $\mathcal{M}_{\Sigma} = \{\mu_e^1, \dots, \mu_e^N\}$ of all different values of μ_e on Σ . Moreover we introduce the sets $\mathcal{I}_{\mu} = \{1 \leq i \leq N: \mu_{e|\Sigma_i} \stackrel{\pm}{=} \mu\}$. Then we denote with Σ_{μ} all facets which have the value μ for μ_e and the according surface fraction with s_{μ} , i.e.

$$\Sigma_{\mu} = \bigcup_{i \in \mathcal{I}_{\mu}} \Sigma_i, \quad s_{\mu} = \sum_{i \in \mathcal{I}_{\mu}} s_i. \quad [53]$$

Doing so, we switch the facet labeling from a consecutive numbering of all facets to values of μ_e . Since $\sum_{\mu \in \mathcal{M}_{\Sigma}} s_{\mu} = 1$, we can introduce the discrete probability density

$$f(\omega) := \sum_{\mu \in \mathcal{M}_{\Sigma}} s_{\mu} \delta(\omega - \mu), \quad [54]$$

where δ is the Dirac-distribution. The charge $Q_{\text{poly}}^{\text{BL}}$ stored in the polycrystalline boundary layer thus rewrites as

$$\begin{aligned} Q_{\text{poly}}^{\text{BL}} &= \sum_{i=1}^N s_i \hat{Q}^{\text{BL}} \left(E - E^{ref} + \frac{1}{e_0} \mu_{e|\Sigma_i} \right) \\ &= \sum_{\mu \in \mathcal{M}_{\Sigma}} s_{\mu} \int_{-\infty}^{\infty} \delta(\omega - \mu) \hat{Q}^{\text{BL}} \left(E - E^{ref} + \frac{1}{e_0} \omega \right) d\omega \\ &= \int_{-\infty}^{\infty} f(\omega) \hat{Q}^{\text{BL}} \left(E - E^{ref} + \frac{1}{e_0} \omega \right) d\omega \\ &= (f * \hat{Q}^{\text{BL}})(E - E^{ref}). \end{aligned} \quad [55]$$

With the convolution operator $*$ we obtain thus a very compact expression for $Q_{\text{poly}}^{\text{BL}}$ in terms of the distribution function $f(\omega)$, which describes the facet density parametrized over the surface potential μ_e . The potential of zero charge $E_{\text{poly}}^{\text{PZC}}$ is thus (implicitly) defined via $(f * \hat{Q}^{\text{BL}})(E - E^{ref}) \stackrel{!}{=} 0$ and the double layer capacity is

$$\begin{aligned} C_{\text{poly}}^{\text{BL}} &= \sum_{i=1}^N s_i \hat{C}^{\text{BL}} \left(E - E^{ref} + \frac{1}{e_0} \mu_e^i \right) \\ &= \int_{-\infty}^{\infty} f(\omega) \hat{C}^{\text{BL}} \left(E - E^{ref} + \frac{1}{e_0} \omega \right) d\omega \\ &= (f * \hat{C}^{\text{BL}})(E - E^{ref}). \end{aligned} \quad [56]$$

Note that \hat{Q}^{BL} and \hat{C}^{BL} remain the non-linear functions described in Section 4.

For realistic polycrystalline electrodes, the Dirac-distribution might smear, whereby f becomes a continuous function. In order to show the consequences of the smearing of the convolution operator $*$ on the non-linear functions of C^{BL} we consider the following example. Let the density f be given by a normal distribution of facets with respect to its mean value $(\mu_e - \bar{\mu}_e) = 0$ and with the standard deviation σ , see Fig. 4. For small standard deviation like $\sigma = 0.025$, the resulting capacity according to 4 is close to the single crystal capacity, see Fig. 4. However, for $\sigma = 0.2$, the local capacity minimum has disappeared and there is only a single capacity maximum. Due to the symmetry of the chosen density $f(\omega)$, the PZC is in either case located at the maximum of the density f . We want to stress, that this particular configuration of facets with a broad scatter of the individual facet properties is very different from the limit related to 5 where on each finite size part of the surface a large number of accordingly small facets are considered.

Next, we want to investigate the effect of a polycrystal surface that is mainly covered by facets near to low index surfaces like (100), (110) and (111). For the low index facets of Ag we chose values of μ_e related to the (negative) work function as given in Table II. To describe a non-ideal Ag polycrystal, we consider a probability density that consists of a superposition of scaled normal distributions around the potentials of the low index facets and a standard deviation small enough, such that the peaks do not overlap, see Fig. 16 where $\sigma = 0.025$ is chosen. The resulting capacity curve remains close to the capacity of an ideal polycrystal with equal surface fractions $s_i = \frac{1}{3}$ for $i = 1, 2, 3$. Moreover, we perturb the configuration such that an equi-distribution in a 1 V potential range is superimposed in the probability

¹In the case $d^{\text{facet}} \rightarrow 0$ the analogous result holds true, due to 5 and 34.

²This situation is equivalent to the slightly non-symmetric case $N = 2$ and $s_1 = 5/9, s_2 = 4/9$.

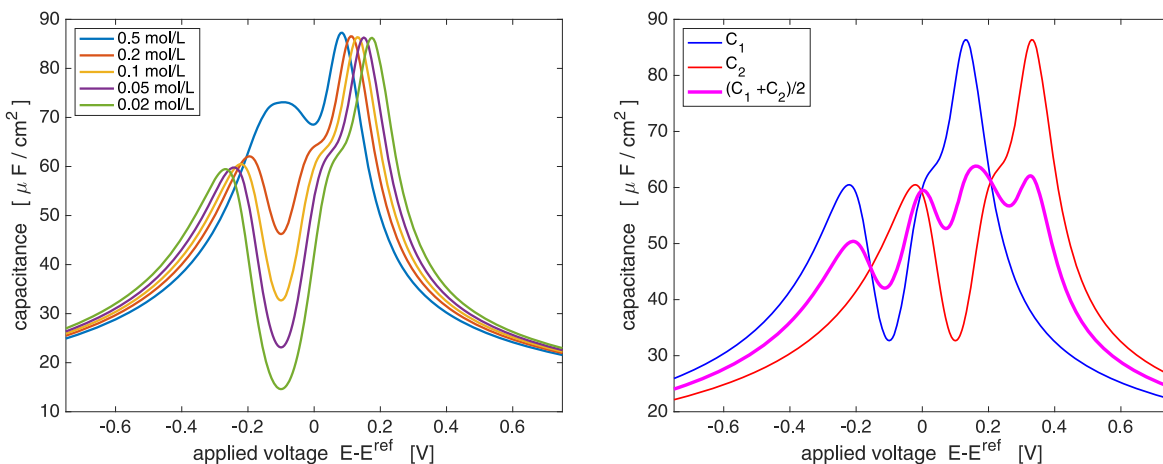


Figure 14. Left: Capacity curves for an adsorbing electrolyte and different bulk electrolyte concentrations where the higher peak at potentials more positive than the PZC is due to adsorption of anions. Right: Construction of the capacity of a polycrystal surface as the sum of the single crystal capacities of the contributing facets weighted by their surface fraction.

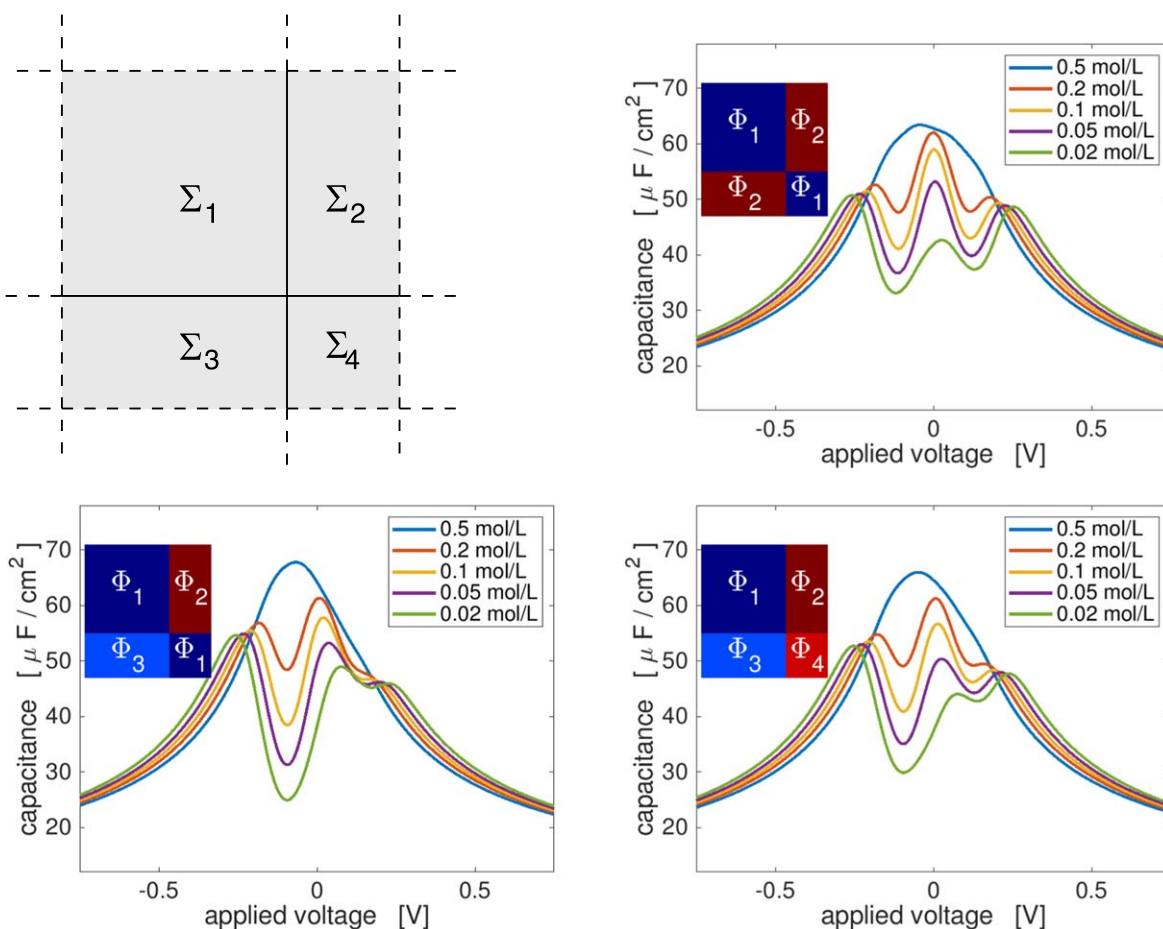


Figure 15. Top left: surface pattern as used in the 3D-FEM simulations of Section 6.3. Top right and bottom row: capacity curves, when assigning the indicated different boundary values on the facets.

density. As a result, we obtain a much more smooth capacity curve. The pure equi-distribution for $\omega(u)$ results in a capacity similar to the normal distribution with large standard deviation.

Conclusions

The double layer model^{16,17,19} is build on a thermodynamically consistent generalized Nernst-Planck model and serves as the

Table II. Recommended values for the electron work function on Ag surfaces according to Ref. 24.

surface	(110)	(100)	(111)
work function	4.10 eV	4.36 eV	4.53 eV
$\mu_e - \bar{\mu}_e$	+0.2 eV	-0.06 eV	-0.23 eV

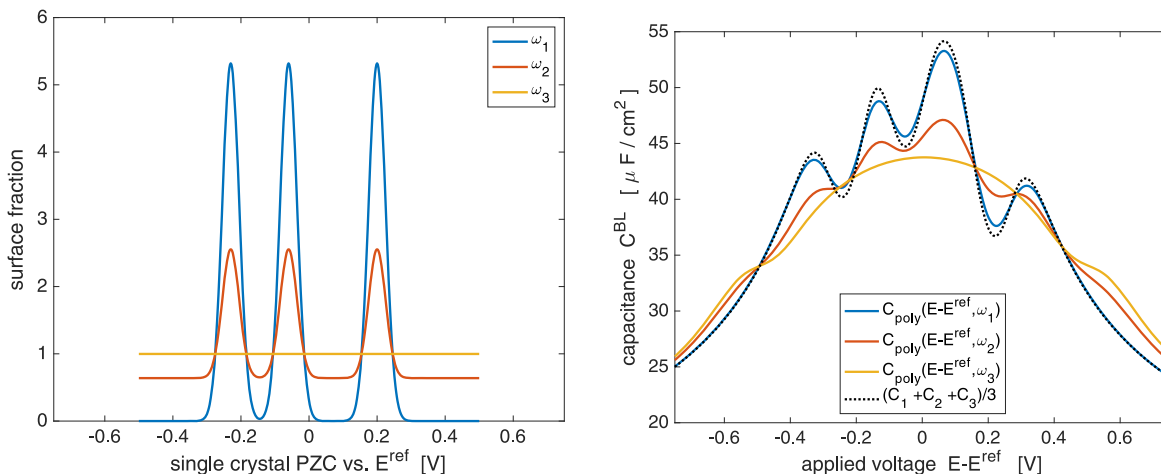


Figure 16. Left: different probability densities describing the surface chemical potential of electrons on a Ag-polycrystal where the surface is covered by facets close to the three low index facets (100), (110) and (111) (blue), the low index facets and additionally an equi-distribution other facets (red), an a pure equi-distribution of facets (yellow). Right: Capacity curves for the respective densities (solid —) and capacity of the ideal polycrystal of only the three low index facets with equal surface fraction (dotted line ...).

theoretical basis of this work. In Ref. 17 it was successfully validated against the most reliable experimental data of single crystal capacitance.^{6–8} This validation now allows to turn the attention from the single crystal to the less well defined conditions of polycrystalline surfaces. By the approach of numerically solving improved Poisson-Boltzmann problems for patterned surfaces, simple representations for the differential capacitance of polycrystalline solid metal electrode surfaces in terms of single crystal capacitance have been obtained. While for a not too small facet size parameter d^{facet} , the result for the capacity of a polycrystalline surface is the expected surface fraction weighted average, some caution is required when considering PZC. Due to the non-linearity in the relation between applied potential and boundary layer charge, the PZC is not given by a weighted average and moreover, it also varies with the electrolyte concentration. The result for $d^{\text{facet}} \rightarrow 0$ can be interpreted in the way that for an amorphous solid material or a liquid material the surface is inhomogeneous on an infinitesimal scale such that the surface properties for each point are independent. Both limits, for large and for small facet size, allow a to get rather clear picture of the electrochemical double layer at patterned surfaces like polycrystal surfaces. Moreover, the results justify the simple correction for rough surfaces by a multiplication with a single geometry dependent factor. In the intermediate cases, where the facets diameters are in the order of 1 [nm], the capacitance of a polycrystalline surface has to be determined from spatially resolved numerical simulation in 2D or 3D and the results depend on the actual geometric surface pattern.

The results obtained here are in rather close resemblance to previous results of Refs. 13, 14 where similar to 3, the capacitance of the polycrystal is given as a surface fraction weighted sum of single crystal capacitances. However, criteria about the applicability of such representations are not directly comparable, since they depend on quantities related to a different model which are not applicable in the context of this work. Spatially resolved and linearized Gouy-Chapman-Stern models were analyzed in Ref. 15 to derive that in the case of sufficiently large differences between the μ_e -values, the

facet size has to be small compared to a length which is related to an inner-layer or Helmholtz capacitance of the individual facets, i.e. $\varepsilon(4\pi C_{\text{Helmholtz}}^i)^{-1} \ll d^{\text{facet}}$. Here, the lower bound is assumed to be independent of the bulk concentration and in any case to be less than 5 nm in aqueous solution. For small differences in the surface chemical potential of the electrons,¹⁵ derives $L^{\text{Debye}} \ll d^{\text{facet}}$ as the sufficient and necessary condition for the applicability of 3. We do not derive a similar criterion here, because one can easily see that the

difference between the two opposite limit Eqs. 3 for $C_{\text{poly},\infty}^{\text{BL}}$ and 5 for $C_{\text{poly},0}^{\text{BL}}$ vanishes quadratically for small difference of the μ_e values, leaving no space for the intermediate cases.

Another interesting aspect of the approach followed here is the possibility to develop a stochastic description of complex polycrystalline surfaces. The results indicate that assembly of an electrode from a huge number of particles with different properties can be represented by a distribution function with a large standard deviation. As a consequence, the capacity of such a surface does not show the typical single crystal camel shape or multiple clearly separated maxima but a rather constant capacity over a broader potential range. In light of this result, the function of supercapacitors can be explained by the inhomogeneity of the fine faceted granular electrode surface.

Outlook. In the modeling of the patterned surfaces with finite facet size parameter d^{facet} , we neglected distinguished contributions from the facet boundary lines. While the according effects on the capacity might be neglected for large enough facets, accurate description of the finite size facet structure might require an extension of the underlying thermodynamic continuum model to line thermodynamics.

The modeling framework applied within this work strictly distinguishes between a universal and a material dependent part. The constitutive functions for the material modeling were chosen here with the emphasis on simplicity. Various extensions of the material model are possible, as for example different concepts of incompressibility, different relations between solvation number and partial volume of solvated ions, concentration dependent dielectric susceptibility. Moreover, the surface model only contains entropic interaction of the ions. Considering also e.g. enthalpic interactions is in principle possible, however it would lead relations between y_{α} and the surface chemical potential μ_{α} that are implicit. Partial charge transfer is possible within the model framework. It entails adsorbed species on the surface with fractional charge number. However, systematic investigations how the (surface) solvation number, the partial molar volume (or area), and the charge number of the ions are related to each other are yet outstanding.

Surface reactions like solvation shell stripping of adsorbed ions can be included into the presented models for polycrystalline surfaces in a straightforward manner. The same also holds true for electron transfer reactions, as long as the reaction products do not leave the surface. In the presence of Faradaic currents additional length scales for the

non-equilibrium transport of ions have to be taken into account. In non-equilibrium, surface roughness on larger length scales might lead to interactions of bulk transport and layer charging causing deviations from ideal behavior of perfectly plain surfaces.

ORCID

Rüdiger Müller  <https://orcid.org/0000-0003-2643-722X>

Jürgen Fuhrmann  <https://orcid.org/0000-0003-4432-2434>

Manuel Landstorfer  <https://orcid.org/0000-0002-0565-2601>

References

1. A. J. Bard and L. R. Faulkner, *Electrochemical Methods: Fundamentals and Applications* (Wiley, New York) (2000).
2. J. O'M. Bockris, A. K. N. Reddy, and M. E. Gamboa-Aldeco, *Modern Electrochemistry 2A: Fundamentals of Electrode Processes* (Kluwer, New York) (2000).
3. J. Newman and K. E. Thomas-Alyea, *Electrochemical Systems* (Wiley, Hoboken, NJ) (2004).
4. J. Hölzl and F. K. Schulte, "Work function of metals." *Solid Surface Physics*, ed. J. Hölzl, F. K. Schulte, and H. Wagner (Springer, Berlin, Heidelberg) p. 1 (1979).
5. S. Trasatti and L. M. Doubova, "Crystal-face specificity of electrical double-layer parameters at metal/solution interfaces." *J. Chem. Soc., Faraday Trans.*, **91**, 3311 (1995).
6. G. Valette, "Double layer on silver single-crystal electrodes in contact with electrolytes having anions which present a slight specific adsorption: Part I. the (110) face." *J. Electroanal. Chem.*, **122**, 285 (1981).
7. G. Valette, "Double layer on silver single crystal electrodes in contact with electrolytes having anions which are slightly specifically adsorbed: Part II. the (100) face." *J. Electroanal. Chem.*, **138**, 37 (1982).
8. G. Valette, "Double layer on silver single crystal electrodes in contact with electrolytes having anions which are slightly specifically adsorbed: Part III. the (111) face." *J. Electroanal. Chem.*, **269**, 191 (1989).
9. D. C. Grahame, "The electrical double layer and the theory of electrocapillarity." *Chem. Rev.*, **41**, 441 (1947).
10. M. A. Vorotyntsev, "Modern state of double layer study of solid metals." *Modern Aspects of Electrochemistry*, ed. J. O'M. Bockris, B. E. Conway, and R. E. White (Springer US, Boston, MA) 17, p. 131 (1986).
11. A. N. Frumkin, "The dependence of the double layer structure on the nature of the metal surface." *J. Res. Inst. Hokkaido Univ.*, **15**, 61 (1967).
12. G. Valette and A. Hamelin, "Structure et propriétés de la couche double électrochimique à l'interphase argent/solutions aqueuses de fluorure de sodium." *J. Electroanal. Chem.*, **45**, 301 (1973).
13. I. A. Bagotskaya, B. B. Damaskin, and M. D. Levi, "The influence of crystallographic inhomogeneity of a polycrystalline electrode surface on the behavior of the electric double-layer." *J. Electroanal. Chem.*, **115**, 189 (1980).
14. M. A. Vorotyntsev, "Capacitance characteristics of a polycrystalline electrode in contact with a surface-inactive electrolyte solution. influence of the size of surface crystal faces." *J. Electroanal. Chem.*, **123**, 379 (1981).
15. M. A. Vorotyntsev, "The capacity of an electrode consisting of uniform fragments with different electrochemical properties (approximation of linear screening in the diffuse layer)." *Sov. Electrochem.*, **17**, 835 (1981).
16. W. Dreyer, C. Guhlke, and R. Müller, "Overcoming the shortcomings of the Nernst-Planck model." *Phys. Chem. Chem. Phys.*, **15**, 7075 (2013).
17. M. Landstorfer, C. Guhlke, and W. Dreyer, "Theory and structure of the metal-electrolyte interface incorporating adsorption and solvation effects." *Electrochim. Acta*, **201**, 187 (2016).
18. W. Dreyer, C. Guhlke, M. Landstorfer, and R. Müller, "New insights on the interfacial tension of electrochemical interfaces and the Lippmann equation." *Eur. J. Appl. Math.*, **29**, 708 (2018).
19. W. Dreyer, C. Guhlke, and R. Müller, "Bulk-surface electro-thermodynamics and applications to electrochemistry." *Entropy*, **20**, 939 (2018).
20. M. S. Kilic, M. Z. Bazant, and A. Ajdari, "Steric effects in the dynamics of electrolytes at large applied voltages. I. double-layer charging." *Phys. Rev. E*, **75**, 021502 (2007).
21. T. Pajkossy, "Impedance of rough capacitive electrodes." *J. Electroanal. Chem.*, **364**, 111 (1994).
22. A. Sommerfeld, "Zur Elektronentheorie der Metalle auf Grund der Fermischen Statistik." *Zeitschrift für Physik*, **47**, 1 (1928).
23. J. O'm. Bockris, M. A. V. Devanathan, K. Müller, and J. A. V. Butler, "On the structure of charged interfaces." *Proc. R. Soc. Lond.*, **274**, 55 (1963).
24. G. N. Derry, M. E. Kern, and E. H. Worth, "Recommended values of clean metal surface work functions." *J. Vac. Sci. Technol. A*, **33**, 060801 (2015).